kinase, cAMP-dependent, regulatory type 1,α) and *PDE4D* (phosphodiesterase 4D, cAMP-specific) involved in the cAMP-mediated G protein-coupled receptor (GPCR) signaling cascade (3–5). *PRKAR1A* consists of 11 exons and encodes type 1α regulatory subunit (RIα) of protein kinase A (PKA) with a dimerization domain, an inhibitory site, and two cAMP-binding domains A and B (6). The PKA holoenzyme is a tetramer consisting of two regulatory subunits and two catalytic subunits, and cooperative binding of two cAMP molecules to each regulatory subunit leads to the dissociation of the catalytic subunits from the regulatory subunits (7). The regulatory subunit-associated catalytic subunits remain inactive, whereas the free catalytic subunits released from the regulatory subunits can phosphorylate a variety of substrate proteins including the cAMP-responsive element (CRE)-binding (CREB) protein (7, 8). It is likely, therefore, that the *PRKAR1A* mutations hinder the cAMP-mediated dissociation of the catalytic subunits from the regulatory subunits, thereby leading to reduced PKA signaling (3). *PDE4D* comprises 15 exons and encodes cAMP-dependent phosphodiesterase 4D (PDE4D) that regulates intracellular cAMP concentrations by converting cAMP to AMP (9). Thus, the *PDE4D* mutations appear to result in desensitization to cAMP because of persistently elevated intracellular cAMP concentrations, thereby affecting the cAMP-mediated GPCR signaling cascade (4). However, functional studies have been performed only for the *PRKAR1A* p.R368X mutation that resides on the last exon and is predicted to escape nonsense-mediated mRNA decay (3), whereas protein modeling analysis argues for the pathological consequences of the remaining *PRKAR1A* and *PDE4D* mutations (4, 5).

Notably, nine of 10 *PRKAR1A* mutation-positive patients and two of seven *PDE4D* mutation-positive patients identified to date exhibit resistance to PTH and/or TSH. Such clinical findings, *i.e.* acrodysostosis plus hormone resistance, overlap with those of pseudohypoparathyroidism type Ia (PHP-Ia), because PHP-Ia is associated with Albright's hereditary osteodystrophy (AHO) reminiscent of acrodysostosis and resistance to several hormones such as PTH and TSH. Indeed, although acrodysostosis and AHO have been classified as different skeletal disorders (2), it is often difficult to distinguish between acrodysostosis and AHO on the basis of clinical and radiological findings (10). Consistent with such phenotypic similarities, PHP-Ia is primarily caused by heterozygous loss-of-function mutations of *GNAS* (the stimulatory G protein α-subunit) (11) that resides in the upstream of *PRKAR1A* and *PDE4D* on the cAMP-mediated GPCR signaling cascade.

Here, we report on a novel *de novo PRKAR1A* mutation and its functional consequence in a patient with acrodysostosis and hormone resistance and discuss phenotypic findings in patients with *PRKAR1A*, *PDE4D*, and *GNAS* mutations.

Patients and Methods

Case report

This Japanese female patient was born to nonconsanguineous parents at 38 wk of gestation. At birth, her length was 46.5 cm (−0.75 SD) and her weight 1.81 kg (−2.8 SD). Neonatal screening tests were normal. Her gross motor milestones were somewhat delayed, with sitting alone without support at 10 months and walking alone at 21 months of age. Her stature remained below −2.0 SD of the mean.

At 3 yr and 10 months of age, she was referred to us because of short stature. Her height was 86.9 cm (−3.1 SD) and her weight 10.6 kg (−2.3 SD). She exhibited round face, nasal hypoplasia, anteverted nostrils, severe brachydactyly of the hands, and mild developmental retardation, and hand roentgenograms showed generalized shortening of the tubular bones with cone shaped epiphyses (Fig. 1A). Brain computerized tomography showed neither sc nor intracranial calcifications. Biochemical and endocrine studies revealed 1) increased serum PTH and plasma cAMP values and normal serum calcium, phosphate, and vitamin D values; 2) decreased urine calcium/creatinine ratio and normal percent tubular reabsorption of phosphate; 3) slightly elevated serum TSH value and normal free T_4 value; 4) age-appropriate serum LH and FSH values; and 5) normal GH response to GHRH stimulation (Table 1). Thus, she was suspected as having acrodysostosis with mild resistance to PTH and TSH.

The parents showed neither brachydactyly nor abnormal endocrine findings (Table 1), although the mother had short stature (144 cm, −2.6 SD).

Molecular and functional studies

We performed 1) direct sequencing for coding exons and their splice sites of *PRKAR1A*, *PDE4D*, and *GNAS*; 2) methylation analysis for four differentially methylated regions (DMR) around *GNAS*; 3) parental testing by microsatellite genotyping; 4) conservation of a substituted amino acid; 5) the forskolin-induced PKA activity of lymphoblastoid cell lines in terms of the phosphorylation status of the CREB protein using Western blot analysis; and 6) forskolin-induced PKA activity using HEK293 cells expressing the wild-type and the mutant proteins. The primers used in this study are shown in Supplemental Table 1, and the detailed methods are described in Supplemental Methods (published on The Endocrine Society's Journals Online web site at http://jcem.endojournals.org).

Results

Analysis of *PRKAR1A*, *PDE4D*, and *GNAS*

No pathological mutation was found for *PDE4D* and *GNAS*, nor was an aberrant methylation pattern detected for the DMR around *GNAS*. By contrast, a novel heterozygous missense mutation (c.715A→G; p.T239A)

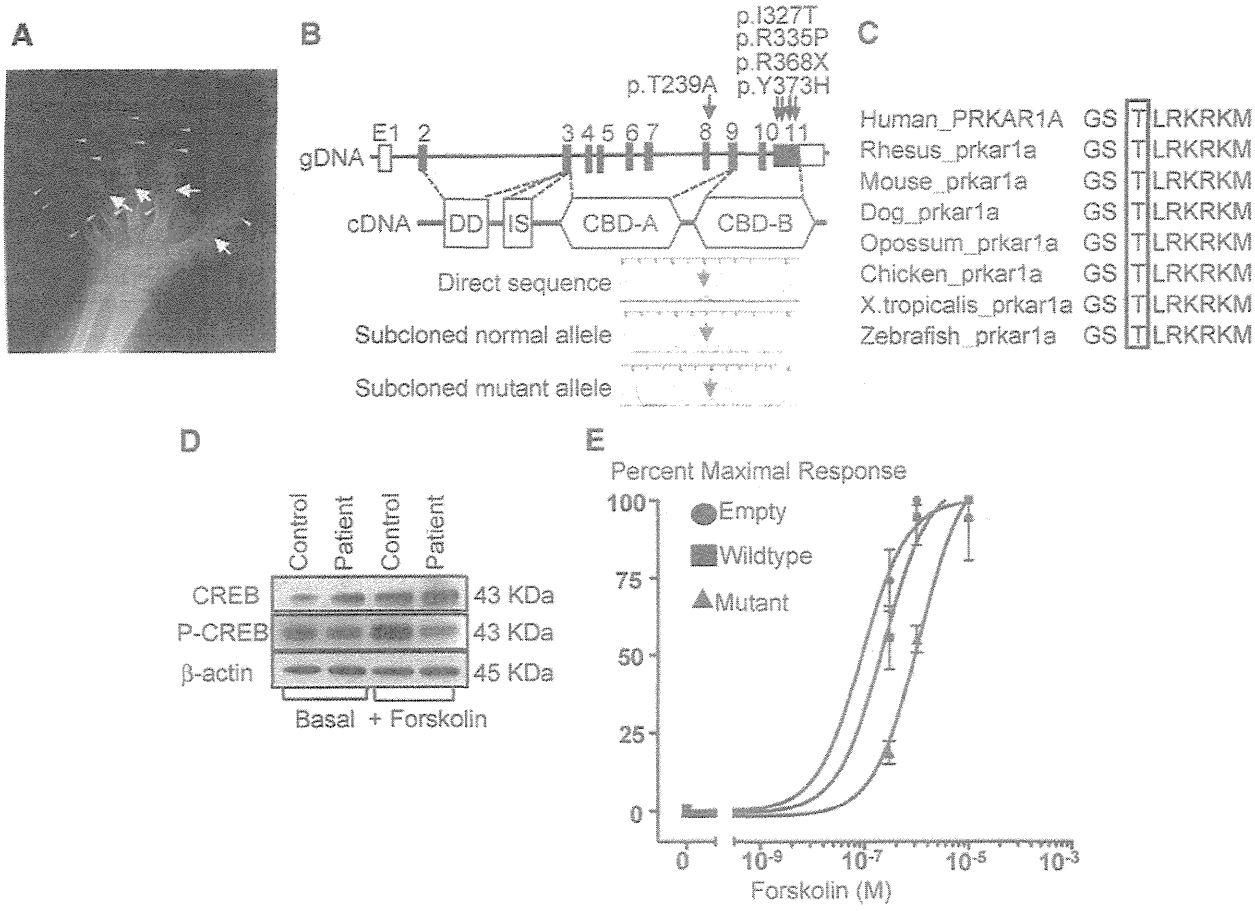

FIG. 1. Representative clinical and experimental findings of this patient. A, Radiograph of the left hand at 3 yr and 10 months of age. Note the shortening of all tubular bones with cone-shaped epiphyses (*arrows*) and early infusions (*arrowheads*). B, The structure of *PRKAR1A* and the position of the mutations identified. The *black and white boxes* on genomic DNA (gDNA) denote the coding regions on exons 2–11 and the untranslated regions, respectively. *PRKAR1A* encodes a dimerization domain (DD), an inhibitory site (IS), and two cAMP-binding domains A and B (CBD-A and -B). A missense mutation (p.T239A) was identified on exon 8 for the cAMP-binding domain A of this patient, whereas the previously described one nonsense and three missense mutations have been found on exon 11 for cAMP-binding domain B (3–5). C, Amino acid sequence of PRKAR1A. Note that the T239 residue is well conserved among species. D, Representative results of Western blot analysis for lymphoblastoid cell lines of the patient and a control subject. The cells were collected before (basal) and after stimulation with 10 μM forskolin. The samples were probed with antibodies for phospho-CREB protein (Ser 133) (P-CREB) and CREB protein, together with those for β-actin used as an internal control. E, Transactivating activities of the wild-type and the mutant PRKAR1A for the CRE-luc reporter. HEK293 cells were transfected with an empty expression vector or with vectors containing either the wild-type PRKAR1A or the p.T239A mutant. Samples were treated with various concentrations of forskolin. The values (percentages to the maximal CRE-luciferase activity) are expressed as the mean ± SE. Curves are fitted with sigmoidal dose-response models. In cells expressing the mutant protein, forskolin induced a concentration-dependent increase in CRE-luciferase activity, yet with a shift to the right in the dose-response curve. The EC_{50} values were significantly higher in the cells expressing the mutant protein than those expressing the wild-type protein ($P < 0.001$). The results are obtained from three independent experiments.

was identified on exon 8 at the cAMP-binding site A of *PRKAR1A* (Fig. 1B). This mutation was absent from her parents and 100 Japanese control subjects.

Parental testing

Microsatellite genotyping data were consistent with paternity as well as maternity of the parents (Supplemental Table 2).

Functional characterization of the mutant *PRKAR1A*

The T239 residue was well conserved among species (Fig. 1C). Protein modeling analysis indicated that the p.T239A resulted in loss of the hydrogen bond between the M236 and the T239 residues and in aberration of the random coils in the mutant PRKAR1A protein, although there was no gross conformational alteration affecting α-helices and β-strands (Supplemental Fig. 1). Western blot analysis indicated obviously reduced forskolin-induced CREB protein phosphorylation in the presence of the apparently normal amount of CREB protein in the lymphoblastoid cell line of this patient (Fig. 1D). Similarly, forskolin-induced PKA activity was significantly lower in the HEK293 cells expressing the mutant PRKAR1A protein than in those expressing the wild-type protein (Fig. 1E).

TABLE 1. Clinical and laboratory data of the patient and her parents

	Patient	Father	Mother[a]
Age (yr)	3 10/12	31	30
Height (cm) (SDS)	**86.9** (−3.1)	177 (+1.1)	**144** (−2.6)
Weight (kg) (SDS)	**10.9** (−2.3)	**89 (+2.5)**	45[b]
Blood			
Intact PTH (pg/ml)	**128** (10–65)	42 (10–65)	23 (10–65)
Calcium (mg/dl)	9.4 (8.5–10.2)	9.4 (8.5–10.2)	9.0 (8.5–10.2)
Phosphate (mg/dl)	5.6 (3.5–5.9)	3.2 (2.4–4.3)	3.6 (2.4–4.3)
25-Hydroxyvitamin D (ng/ml)	26 (7–41)	NA	NA
TSH (mU/liter)	**7.2** (0.5–5.0)	1.7 (0.5–5.0)	1.2 (0.5–5.0)
Free T_4 (ng/ml)	1.2 (0.9–1.6)	1.3 (0.9–1.6)	1.1 (0.9–1.6)
LH (IU/liter)	<0.1 (<0.7)	4.1 (0.8–5.7)	0.17 (1.8–10.2)[c]
FSH (IU/liter)	0.9 (0.6–5.3)	6.6 (2.0–8.3)	0.07 (3.0–14.7)[c]
GH (ng/ml) stimulated[d]	19.5 (>9)	NA	NA
cAMP (pmol/ml)	**39.6** (6.4–20.8)	NA	NA
Urine			
Calcium/creatinine ratio	**0.04** (0.13–0.25)	NA	NA
% TRP	91 (81.3–93.3)	NA	NA

The values in *parentheses* indicate the SD score (SDS) for heights and weights and the age-and sex-matched reference blood and urine hormone and laboratory data. The conversion factors to the SI unit are as follows: intact PTH, 1.0 (nanograms per liter); serum calcium, 0.25 (millimoles per liter); serum phosphate, 0.3229 (millimoles per liter); 25-hydroxyvitamin D, 2.496 (nanomoles per liter); free T_4, 12.9 (picomoles per liter); GH, 1.0 (micrograms per liter); and cAMP, 1.0 (nanomoles per liter). Hormone values have been evaluated by the age- and sex-matched Japanese reference data; abnormal data are in *bold*. NA, Not available; TRP, tubular reabsorption of phosphate.

[a] During the second trimester of pregnancy.

[b] Not assessed because of pregnancy.

[c] Low LH/FSH values are consistent with pregnant status of the mother (18).

[d] Blood sampling during the provocation tests were done at 0, 30, 60, 90, and 120 min after GHRH stimulation (1 μg/kg).

Discussion

We identified a novel *de novo* heterozygous *PRKAR1A* mutation in a patient with acrodysostosis and mild resistance to PTH and TSH. In this regard, several findings are noteworthy. First, although the phenotypic findings of this patient are similar to those of PHP-Ia, the severe skeletal lesion would be regarded as acrodysostosis rather than AHO. Consistent with this, a mutation was identified in *PRKAR1A* rather than *GNAS*. Second, the p.T239A was present at the cAMP-binding domain A, in contrast to the previously reported *PRKAR1A* mutations that were invariably located at the cAMP-binding domain B (3–5). In this regard, because cAMP binds first to the binding domain B and then to the binding domain A, it has been suggested that the binding domain B acts as the gatekeeper of the PKA activation, and that the binding domain A is relatively inaccessible to cAMP (8). Despite such a hierarchical phenomenon, this study indicates that mutations at the cAMP-binding domains A and B lead to a similar clinical phenotype. Third, functional analyses showed obviously reduced PKA signaling of the mutant PRKAR1A protein. Thus, the p.T239A mutation appears to impair the dissociation of the catalytic subunits from the RIα regulatory subunits, thereby leading to the reduced GPCR signaling, as has been stated by the functional studies for the p.R368X mutation (3). Although the underlying factors remains to be elucidated, loss of the hydrogen bond and aberration of the random coils in the mutant PRKAR1A protein may be relevant to this functional alteration.

To date, *GNAS*, *PRKAR1A*, and *PDE4D* mutations have been identified in patients with overlapping skeletal and endocrine phenotypes (3–5). It appears, however, that *GNAS* abnormalities usually lead to relatively mild skeletal phenotype and clinically discernible hormone resistance, whereas *PRKAR1A* and *PDE4D* mutations usually result in relatively severe skeletal lesion and mild or absent hormone resistance. In this regard, it is predicted in patients with maternally derived *GNAS* mutations that normally functioning *GNAS* is absent from several tissues including renal proximal tubules where *GNAS* is paternally imprinted and is present in a single copy in other tissues including skeletal tissues where *GNAS* is biparentally expressed (11, 12). By contrast, it is likely in patients with *PRKAR1A* and *PDE4D* mutations that normally functioning *PRKAR1A* and *PDE4D* are present in a single copy in all the tissues because of the absence of DMR around these genes (13). Such a difference in the functional gene dosage in several *GNAS*-imprinted tissues may more or less be relevant to the prevalent hormone resistance in *GNAS* mutations. Furthermore, because there are four genes encoding the regulatory subunits of PKA (RIa, RIb,

RIIa, and RIIb) and three genes encoding the catalytic subunits (14), such redundancy would also be related to the apparently mild hormone resistance in *PRKAR1A* mutations. However, these factors are unlikely to account for the apparently severe skeletal lesion in *PRKAR1A* and *PDE4D* mutations. Furthermore, although aberrant signaling via PTHrP receptor belonging to the GPCR families may play an important role in the development of skeletal lesions in *PRKAR1A* mutations, this perturbation is also relevant to the occurrence of skeletal lesions in *GNAS* abnormalities (15). Thus, there may be a hitherto unknown factor involved in the development of severe skeletal phenotype in *PRKAR1A* and *PDE4D* mutations. Notably, hormone resistance is apparently infrequent in acrodysostosis (2). It remains to be clarified whether acrodysostosis with and without hormone resistance may represent genetically heterogeneous conditions, and whether hormone resistance may have been overlooked or remained at a subclinical level in a certain fraction of patients with *PRKAR1A* and *PDE4D* mutations.

For *PRKAR1A*, more than 100 different mutations have been identified in Carney complex with multiple neoplasias and lentiginosis (16). Because most mutations reported in Carney complex are frameshift, nonsense, and splice mutations that are predicted to undergo nonsense-mediated mRNA decay and cause *PRKAR1A* haploinsufficiency, they would result in the increased amount of the free-lying intracellular catalytic subunits, leading to excessive PKA signaling in target tissues (16, 17). Furthermore, other types of mutations have also been identified in Carney complex, such as missense mutations at the cAMP-binding domain A (*e.g.* p.D183Y and p.A213D) and an in-frame deletion of 53 amino acids from the binding domain A (c.708 + 1 g→t) (16). Thus, in conjunction with the results of this study, we presume that *PRKAR1A* mutations can cause a mirror image of disorders in terms of the PKA activity, *i.e.* Carney complex resulting from defective association between the regulatory and the catalytic subunits and acrodysostosis with hormone resistance ascribed to impaired dissociation between the two subunits.

In summary, we identified a heterozygous *PRKAR1A* mutation affecting cAMP-mediated GPCR signaling in a patient with acrodysostosis with hormone resistance. Additional studies will permit a better clarification of the underlying causes in acrodysostosis with and without hormone resistance.

Acknowledgments

We thank Professor N. Matsuura (Seitoku University) and Dr. S. Narumi (Keio University School of Medicine) for fruitful discussion. We are grateful to Drs. N. Katsumata and S. Takada and Ms. A. Nagashima, T. Tanji, E. Suzuki, and I. Kobayashi (National Research Institute for Child Health and Development) for their technical assistance.

Address all correspondence and requests for reprints to: Dr. Tsutomu Ogata, Department of Pediatrics, Hamamatsu University School of Medicine, Hamamatsu 431-3192, Japan. E-mail: tomogata@hama-med.ac.jp; or Dr. Maki Fukami, Department of Molecular Endocrinology, National Research Institute for Child Health and Development, Tokyo 157-8535, Japan. E-mail: mfukami@nch.go.jp.

This work was supported by the Grant-in-Aid for Scientific Research on Innovative Areas (22132004) from the Ministry of Education, Culture, Sports, Science, and Technology; by the Grant-in-Aid for Scientific Research (B) (23390249) from the Japan Society for the Promotion of Science; and by grants from the Foundation for Growth Science, from the National Center for Child Health and Development (23A-1), and from the Ministry of Health, Labor, and Welfare.

Disclosure Summary: The authors declare no conflict of interest.

References

1. **Wilson LC, Oude Luttikhuis ME, Baraitser M, Kingston HM, Trembath RC** 1997 Normal erythrocyte membrane Gsα bioactivity in two unrelated patients with acrodysostosis. J Med Genet 34:133–136
2. **Graham Jr JM, Krakow D, Tolo VT, Smith AK, Lachman RS** 2001 Radiographic findings and Gs-α bioactivity studies and mutation screening in acrodysostosis indicate a different etiology from pseudohypoparathyroidism. Pediatr Radiol 31:2–9
3. **Linglart A, Menguy C, Couvineau A, Auzan C, Gunes Y, Cancel M, Motte E, Pinto G, Chanson P, Bougnères P, Clauser E, Silve C** 2011 Recurrent PRKAR1A mutation in acrodysostosis with hormone resistance. N Engl J Med 364:2218–2226
4. **Lee H, Graham Jr JM, Rimoin DL, Lachman RS, Krejci P, Tompson SW, Nelson SF, Krakow D, Cohn DH** 2012 Exome sequencing identifies PDE4D mutations in acrodysostosis. Am J Hum Genet 90:746–751
5. **Michot C, Le Goff C, Goldenberg A, Abhyankar A, Klein C, Kinning E, Guerrot AM, Flahaut P, Duncombe A, Baujat G, Lyonnet S, Thalassinos C, Nitschke P, Casanova JL, Le Merrer M, Munnich A, Cormier-Daire V** 2012 Exome sequencing identifies PDE4D mutations as another cause of acrodysostosis. Am J Hum Genet 90:740–745
6. **Scott JD** 1991 Cyclic nucleotide-dependent protein kinases. Pharmacol Ther 50:123–145
7. **Taskén K, Skålhegg BS, Solberg R, Andersson KB, Taylor SS, Lea T, Blomhoff HK, Jahnsen T, Hansson V** 1993 Novel isozymes of cAMP-dependent protein kinase exist in human cells due to formation of RIα-RIβ heterodimeric complexes. J Biol Chem 268:21276–21283
8. **Kim C, Xuong NH, Taylor SS** 2005 Crystal structure of a complex between the catalytic and regulatory (RIα) subunits of PKA. Science 307:690–696
9. **Verghese MW, McConnell RT, Lenhard JM, Hamacher L, Jin SL** 1995 Regulation of distinct cyclic AMP-specific phosphodiesterase (phosphodiesterase type 4) isozymes in human monocytic cells. Mol Pharmacol 47:1164–1171
10. **Ablow RC, Hsia YE, Brandt IK** 1977 Acrodysostosis coinciding with pseudohypoparathyroidism and pseudo-pseudohypoparathyroidism. AJR Am J Roentgenol 128:95–99

11. **Weinstein LS, Yu S, Warner DR, Liu J** 2001 Endocrine manifestations of stimulatory G protein α-subunit mutations and the role of genomic imprinting. Endocr Rev 22:675–705
12. **Mantovani G, Bondioni S, Locatelli M, Pedroni C, Lania AG, Ferrante E, Filopanti M, Beck-Peccoz P, Spada A** 2004 Biallelic expression of the Gsα gene in human bone and adipose tissue. J Clin Endocrinol Metab 89:6316–6319
13. **He H, Olesnanik K, Nagy R, Liyanarachchi S, Prasad ML, Stratakis CA, Kloos RT, de la Chapelle A** 2005 Allelic variation in gene expression in thyroid tissue. Thyroid 15:660–667
14. **Foss KB, Landmark B, Skålhegg BS, Taskén K, Jellum E, Hansson V, Jahnsen T** 1994 Characterization of in-vitro-translated human regulatory and catalytic subunits of cAMP-dependent protein kinases. Eur J Biochem 220:217–223
15. **Lanske B, Karaplis AC, Lee K, Luz A, Vortkamp A, Pirro A, Karperien M, Defize LH, Ho C, Mulligan RC, Abou-Samra AB, Jüppner H, Segre GV, Kronenberg HM** 1996 PTH/PTHrP receptor in early development and Indian hedgehog-regulated bone growth. Science 273:663–666
16. **Horvath A, Bertherat J, Groussin L, Guillaud-Bataille M, Tsang K, Cazabat L, Libé R, Remmers E, René-Corail F, Faucz FR, Clauser E, Calender A, Bertagna X, Carney JA, Stratakis CA** 2010 Mutations and polymorphisms in the gene encoding regulatory subunit type 1-α of protein kinase A (PRKAR1A): an update. Hum Mutat 31:369–379
17. **Robinson-White A, Meoli E, Stergiopoulos S, Horvath A, Boikos S, Bossis I, Stratakis CA** 2006 PRKAR1A mutations and protein kinase A interactions with other signaling pathways in the adrenal cortex. J Clin Endocrinol Metab 91:2380–2388
18. **Kronenberg HM, Melmed S, Polonsky KS, Larsen PR** 2008 Endocrine change in pregnancy. In: Braunstein GD, ed. Williams textbook of endocrinology. 11th ed. Philadelphia: Saunders Elsevier; 743

Epigenetics 7:10, 1142-1150; October 2012; © 2012 Landes Bioscience

Paternal uniparental disomy 14 and related disorders

Placental gene expression analyses and histological examinations

Masayo Kagami,[1] Kentaro Matsuoka,[2] Toshiro Nagai,[3] Michiko Yamanaka,[4] Kenji Kurosawa,[5] Nobuhiro Suzumori,[6] Yoichi Sekita,[7] Mami Miyado,[1] Keiko Matsubara,[1] Tomoko Fuke,[1] Fumiko Kato,[1,8] Maki Fukami[1] and Tsutomu Ogata[1,8,*]

[1]Department of Molecular Endocrinology; National Research Institute for Child Health and Development; Tokyo, Japan; [2]Departments of Pathology; National Center for Child Health and Development; Tokyo, Japan; [3]Department of Pediatrics; Dokkyo University School of Medicine; Koshigaya, Japan; [4]Department of Integrated Women's Health; St. Luke's International Hospital; Tokyo, Japan; [5]Division of Medical Genetics; Kanagawa Children's Medical Center; Yokohama, Japan; [6]Department of Obstetrics and Gynecology; Nagoya City University Graduate School of Medicine; Nagoya, Japan; [7]Department of Pathology; Graduate School of Medicine; Osaka University, Osaka, Japan; [8]Department of Pediatrics; Hamamatsu University School of Medicine; Hamamatsu, Japan

Keywords: Upd(14)pat, microdeletion, placenta, expression dosage, histopathology, imprinting

Abbreviations: *PEGs*, paternally expressed genes; *MEGs*, maternally expressed genes; DMRs, differentially methylated regions; IG-DMR, *DLK1-MEG3* intergenic DMR; *RTL1as*, *RTL1* antisense; upd(14)pat, paternal uniparental disomy 14; BWS, Beckwith-Wiedemann syndrome; q-PCR, quantitative real-time PCR; CGH, oligoarray comparative genomic hybridization; LM, light microscopic; EM, electron microscopic; IHC, immunohistochemical

Although recent studies in patients with paternal uniparental disomy 14 [upd(14)pat] and other conditions affecting the chromosome 14q32.2 imprinted region have successfully identified underlying epigenetic factors involved in the development of upd(14)pat phenotype, several matters, including regulatory mechanism(s) for *RTL1* expression, imprinting status of *DIO3* and placental histological characteristics, remain to be elucidated. We therefore performed molecular studies using fresh placental samples from two patients with upd(14)pat. We observed that *RTL1* expression level was about five times higher in the placental samples of the two patients than in control placental samples, whereas *DIO3* expression level was similar between the placental samples of the two patients and the control placental samples. We next performed histological studies using the above fresh placental samples and formalin-fixed and paraffin-embedded placental samples obtained from a patient with a maternally derived microdeletion involving *DLK1*, the IG-DMR, the *MEG3*-DMR and *MEG3*. Terminal villi were associated with swollen vascular endothelial cells and hypertrophic pericytes, together with narrowed capillary lumens. DLK1, RTL1 and DIO3 proteins were specifically identified in vascular endothelial cells and pericytes, and the degree of protein staining was well correlated with the expression dosage of corresponding genes. These results suggest that *RTL1as*-encoded microRNA functions as a repressor of *RTL1* expression, and argue against *DIO3* being a paternally expressed gene. Furthermore, it is inferred that DLK1, DIO3 and, specially, RTL1 proteins, play a pivotal role in the development of vascular endothelial cells and pericytes.

Introduction

Human chromosome 14q32.2 region carries a cluster of imprinted genes including protein coding paternally expressed genes (*PEGs*) such as *DLK1* and *RTL1* (alias *PEG11*) and non-coding maternally expressed genes (*MEGs*) such as *MEG3* (alias *GTL2*) and *RTL1as* (*RTL1* antisense encoding microRNAs).[1,2] The 14q32.2 imprinted region also harbors two differentially methylated regions (DMRs), i.e., the germline-derived primary *DLK1-MEG3* intergenic DMR (IG-DMR) and the postfertilization-derived secondary *MEG3*-DMR.[1,2] Both DMRs are hypermethylated after paternal transmission and hypomethylated after maternal transmission in the body, whereas in the placenta the IG-DMR alone remains as a DMR and the *MEG3*-DMR is rather hypomethylated.[2] We have previously revealed that the hypomethylated IG-DMR and *MEG3*-DMR of maternal origin function as imprinting control centers in the placenta and the body, respectively, and that the IG-DMR functions hierarchically as an upstream regulator for the methylation pattern of the *MEG3*-DMR on the maternally inherited chromosome in the body, but not in the placenta.[3]

*Correspondence to: Tsutomu Ogata; Email: tomogata@hama-med.ac.jp
Submitted: 06/21/12; Revised: 08/20/12; Accepted: 08/22/12
http://dx.doi.org/10.4161/epi.21937

Consistent with these findings, paternal uniparental disomy 14 [upd(14)pat] results in a unique phenotype characterized by facial abnormality, small bell-shaped thorax with coat hanger appearance of the ribs, abdominal wall defects, placentomegaly and polyhydramnios.[2,4] We have studied multiple patients with upd(14)pat and related conditions, such as epimutations of the maternally derived DMRs and various types of microdeletions involving the maternally inherited imprinted region, suggesting that markedly increased *RTL1* expression is the major underlying factor for the development of upd(14)pat-like phenotype.[2] The notion of excessive *RTL1* expression is primarily based on the following mouse data indicating a trans-acting repressor function of *Rtl1as*-encoded microRNAs for *Rtl1* expression: (1) targeted deletion of the maternally derived IG-DMR causes maternal to paternal epigenotypic switch of the imprinted region, with ~4.5 times rather than ~2 times of *Rtl1* expression as well as ~2 times of *Dlk1* expression and nearly absent *Megs* expression, in the presence of two functional copies of *Pegs* and no functional copy of *Megs*[5] and; (2) targeted deletion of the maternally derived *Rtl1as* results in 2.5–3.0 times of *Rtl1* expression, in the presence of a single functional copy of *Rtl1*.[6] Similarly, in the human, typical upd(14)pat phenotype is observed in patients with epimutations that are likely associated with markedly increased *RTL1* expression because of the combination of two functional copies of *RTL1* and no functional copy of *RTL1as*, whereas relatively mild upd(14)pat-like phenotype is found in patients with maternally inherited microdeletions involving *RTL1as* that are likely accompanied by moderately elevated *RTL1* expression because of the combination of a single functional copy of *RTL1* and no functional copy of *RTL1as*.[2]

Human imprinting disorders are usually associated with placental abnormalities. For example, Beckwith-Wiedemann syndrome (BWS) and upd(14)pat are associated with placentomegaly,[4,7] and Silver-Russell syndrome is accompanied by hypoplastic placenta.[8] Similarly, mouse imprinting aberrations also usually affect placental growth and development.[9] In agreement with this, virtually all the imprinted genes studied to date are expressed in the placenta and play a pivotal role in the placental growth and development,[10] although placental structure is more or less different between placental animals.[11]

However, several matters remain to be clarified in upd(14)pat and related conditions. For example, it is unknown whether human *RTL1* expression is actually elevated in the absence of functional *RTL1as*-encoded microRNAs. It is also unknown whether *DIO3* is a *PEG*, although mouse *Dio3* has been shown to undergo partial imprinting.[12] In this regard, while we examined fresh blood cells, cultured skin fibroblasts and formalin-fixed and paraffin-embedded placental and body samples obtained from patients with upd(14)pat-like phenotype, precise assessment of *RTL1* and *DIO3* expression levels was impossible because of extremely low *RTL1* and *DIO3* expression levels in fresh blood cells and cultured skin fibroblasts and poor quality of RNAs extracted from paraffin-embedded tissues.[2,3] In addition, while cSNP genotyping has demonstrated paternal *DLK1* and *RTL1* expression and maternal *MEG3* expression in the body and the placenta,[2,3] no informative cSNP data showing paternal *DIO3* expression have been obtained.[2,3] Furthermore, although standard light microscopic (LM) examinations have been performed using formalin-fixed and paraffin-embedded placental samples, fine placental histopathological studies, such as electron microscopic (EM) examinations and immunohistochemical (IHC) examinations, remain to be performed.

To examine these unresolved matters, fresh placental tissues are highly useful, because precise quantitative real-time PCR (q-PCR) analyses and EM studies can be performed with fresh placentas. Thus, we performed q-PCR analyses and EM studies, as well as IHC studies with RTL1 antibodies produced by ourselves and commercially available DLK1 and DIO3 antibodies, using fresh placental samples obtained from two previously reported patients with prenatally diagnosed upd(14)pat.[13,14] We also performed IHC studies using formalin-fixed and paraffin-embedded placental samples obtained from a previously reported patient with a microdeletion involving *DLK1*, but not *RTL1* and *DIO3*,[2] to compare the placental protein expression levels between upd(14)pat and the microdeletion. Furthermore, we also studied a hitherto unreported patient with an unbalanced translocation involving the 14q32.2 imprinted region, to obtain additional data regarding the *RTL1-RTL1as* interaction and the primary factor for the development of upd(14)pat phenotype.

Results

Patients and samples. This study consisted of three previously reported patients with typical body and placental upd(14)pat phenotype and a normal karyotype (cases 1–3),[2,13-15] and a new patient with various non-specific features and a 46,XX,der(17)t(14;17)(q31;p13) karyotype accompanied by three copies of the distal 14q region and a single copy of the terminal 17p region (case 4) . Clinical phenotypes of cases 1–4 are summarized in **Table S1**. In brief, cases 1 and 2 were suspected to have upd(14)pat phenotype including bell-shaped thorax by prenatal ultrasound studies performed for polyhydroamnios, and were confirmed to have upd(14)pat by microsatellite analysis after birth. Case 3 was found to have typical upd(14)pat phenotype during infancy and was shown to have a maternally derived microdeletion affecting the chromosome 14q32.2 imprinted region. Case 4 had growth failure, developmental delay, multiple non-specific anomalies, and omphalocele. There was no history of polyhydramnios or placentomegaly. Thus, except for omphalocele, case 4 had no upd(14)pat-like phenotype. The parental karyotype was normal, indicating a de novo occurrence of the unbalanced translocation.

We obtained fresh placental samples immediately after birth from prenatally diagnosed cases 1 and 2 for molecular studies using genomic DNA and RNA, and fresh leukocyte samples from cases 1, 2 and 4 and their parents for molecular studies using genomic DNA. The fresh placental samples of cases 1 and 2 were also utilized for histopathological examinations, together with formalin-fixed and paraffin-embedded placental samples of case 3. For controls, we obtained three fresh placentas at 37 weeks of gestation, and fresh leukocytes from three adult subjects; for molecular studies using placentas, we prepared pooled samples

consisting of an equal amount of DNA or RNA extracted from each placenta.

Molecular studies in cases 1 and 2. We performed microsatellite analysis for 19 loci on chromosome 14 and bisulfite sequencing for the IG-DMR (CG4 and CG6) and the *MEG3*-DMR (CG7), using placental and leukocyte genomic DNA samples; while microsatellite analysis had been performed for 15 loci in case 1 and 16 loci in case 2, only leukocyte genomic DNA samples were examined in the previous study.[15] Consequently, we identified two peaks for *D14S609* and single peaks for the remaining loci in case 1 (the combination of paternal heterodisomy and isodisomy), and single peaks for all the examined loci in case 2 (apparently full paternal isodisomy) (**Table S2**). Furthermore, no trace of maternally inherited peak was identified in both placental and leukocyte genomic DNA samples (**Fig. 1**). Bisulfite sequencing showed that both the IG-DMR and the *MEG3*-DMR were markedly hypermethylated in the leukocytes of cases 1 and 2, whereas in the placental samples the IG-DMR was obviously hypermethylated and the *MEG3*-DMR was grossly hypomethylated to an extent similar to that identified in control placentas (**Fig. 2**). Furthermore, q-PCR analysis for placental RNA samples revealed that *DLK1*, *RTL1*, and *DIO3* expression levels were 3.3 times, 6.1 times and 1.9 times higher in the placental samples of case 1 than in the control placental samples, respectively, and were 3.1 times, 9.4 times and 1.7 times higher in the placental samples of case 2 than in the control placental samples, respectively (**Fig. 3A**). By contrast, the expressions of all *MEGs* examined were virtually absent in the placental samples of cases 1 and 2. PCR products were sufficiently obtained after 30 cycles for the fresh placental as well as leukocyte samples, consistent with high quality of DNA and RNA obtained from fresh materials.

Molecular studies in case 3. Detailed molecular findings have already been reported previously.[2] In brief, microsatellite analysis revealed biparentally derived homologs of chromosome 14, and a deletion analysis demonstrated a maternally inherited 108,768 bp microdeletion involving *DLK1*, the IG-DMR, the *MEG3*-DMR, and *MEG3*, but not affecting *RTL1*/*RTL1as*. Since loss of the DMRs causes maternal to paternal epigenotypic alteration,[2] it is predicted that case 3 has a single functional copy of *DLK1* and two functional copies of *RTL1* and *DIO3*, as well as no functional copy of *RTL1as* and other *MEGs*. Bisulfite sequencing showed that both the IG-DMR and the *MEG3*-DMR were markedly hypermethylated in leukocytes, whereas in the formalin-fixed and paraffin-embedded placental samples the IG-DMR was obviously hypermethylated and the *MEG3*-DMR was comprised of roughly two-thirds of hypermethylated clones and roughly one-third of hypomethylated clones. In addition, RT-PCR analysis for such placental samples indicated positive *PEGs* (especially *RTL1*) expression and absent *MEGs* expression. For the formalin-fixed and paraffin-embedded placental samples, PCR products could be obtained only after 35 cycles, because of poor quality (severe degradation) of DNA and RNA.

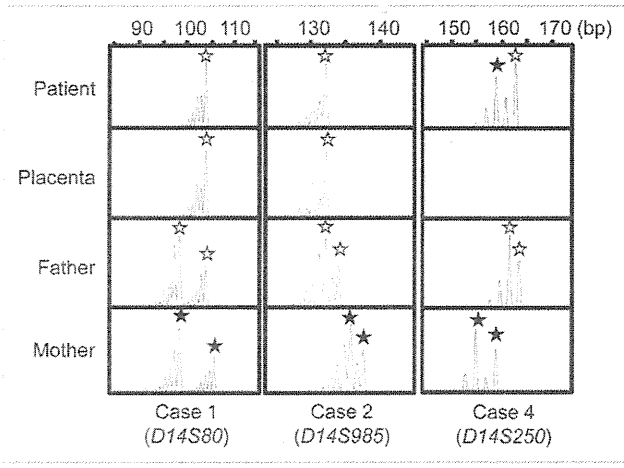

Figure 1. Representative results of microsatellite analysis, using leukocyte genomic DNA samples of the patient and the parents and placental genomic DNA samples. In cases 1 and 2, one of the two paternal peaks is inherited by the patients and the placentas, and no trace of maternal peaks is identified. In case 4, both paternally and maternally derived peaks are found in the patient, with the paternally derived long peak being larger than the maternally inherited short peak.

Molecular findings in case 4. We examined the presence or absence of the 14q32.2 imprinted region on the der(17) chromosome (**Fig. 4**). Oligoarray comparative genomic hybridization (CGH) indicated three copies of a ~19.6 Mb 14q31–qter region, and FISH analysis for four segments around the chromosome 14q32.2 imprinted region delineated positive signals on the der(17) chromosome as well as on the normal chromosome 14 homologs. This demonstrated the presence of the 14q32.2 imprinted region on the der(17) chromosome. In addition, similar oligoarray CGH and FISH analysis revealed loss of a ~455 kb region from the distal chromosome 17p (**Fig. S1**).

Thus, we investigated the parental origin of the translocated 14q distal region. Microsatellite analysis for *D14S250* and *D14S1007* on the translocated 14q distal region delineated biparentally derived two peaks, with paternally derived long PCR products showing larger peaks than maternally derived short PCR products (**Fig. 1**; **Table S2**). Since short products are usually more easily amplified than long products, this indicated paternal

Figure 2 (See opposite page). Bisulfite sequencing analysis of the IG-DMR (CG4 and CG6) and the *MEG3*-DMR (CG7), using leukocyte and placental genomic DNA samples. Filled and open circles indicate methylated and unmethylated cytosines at the CpG dinucleotides, respectively. Upper part: structure of CG4, CG6, and CG7. Pat, paternally derived chromosome; Mat, maternally derived chromosome. The PCR products for CG4 (311 bp) harbor 6 CpG dinucleotides and a G/A SNP (*rs12437020*), those for CG6 (428 bp) carry 19 CpG dinucleotides and a C/T SNP (*rs10133627*) and those for CG7 (168 bp) harbor 7 CpG dinucleotides. Lower part: the results of cases 1, 2, 4 and a control subject. Each horizontal line indicates a single subcloned allele. The control data represent the methylation patterns obtained with a leukocyte genomic DNA sample extracted from a single subject heterozygous for the G/A SNP (*rs12437020*) (body) and those obtained with a pooled DNA sample consisting of an equal amount of genomic DNA extracted from three control placentas homozygous for that SNP.

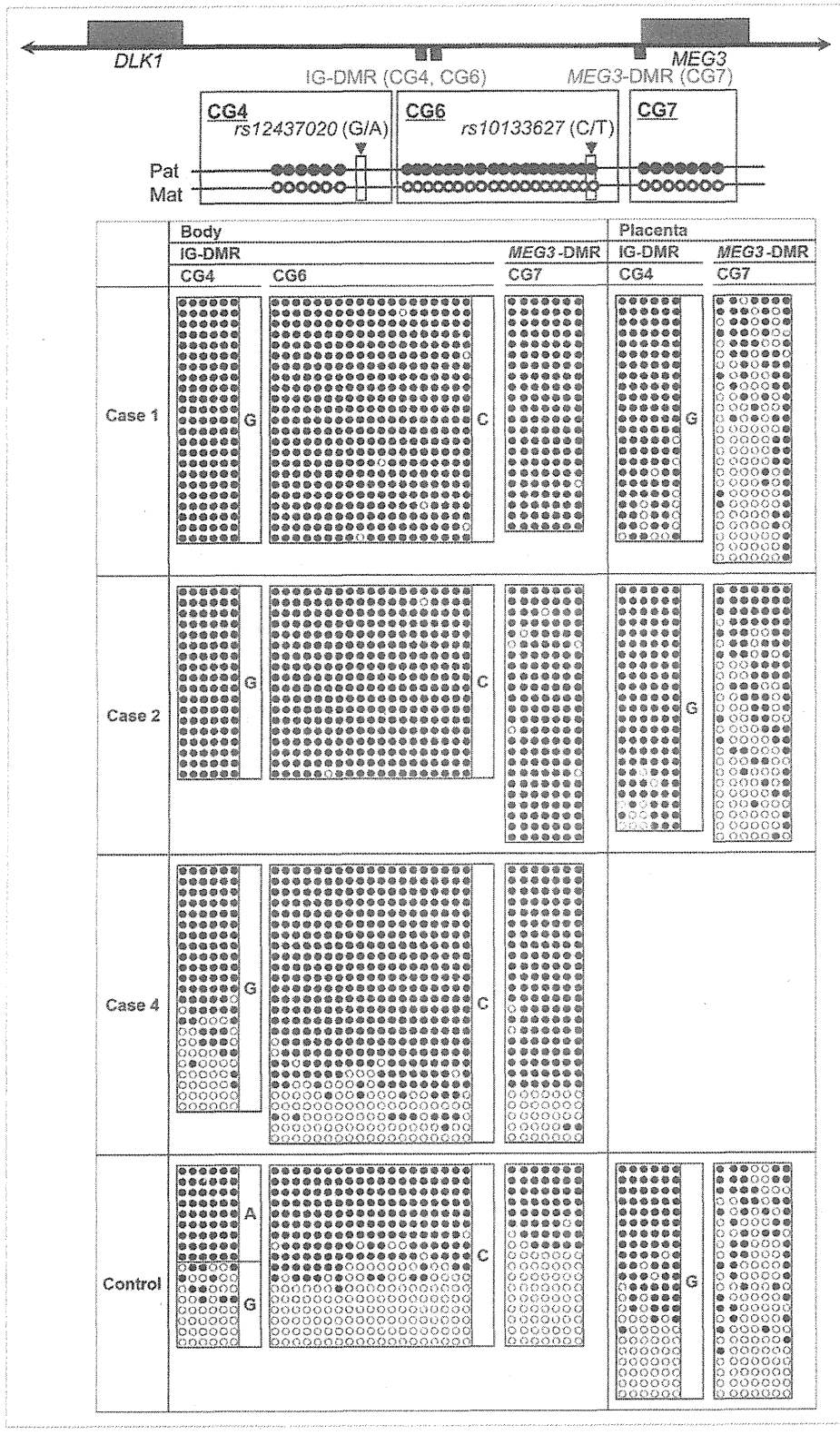

Figure 2. For figure legend, see page 1144.

origin of the der(17) chromosome harboring the chromosome14q32.2 imprinted region. Consistent with this, bisulfite sequencing showed moderate hypermethylation of the IG-DMR and the *MEG3*-DMR (Fig. 2).

Placental histopathological studies. We performed LM and EM studies, and IHC examinations (Fig. 5). LM examinations showed proliferated chorionic villi in cases 1–3. Capillary lumens were irregularly dilated with thickened endothelium in the stem to intermediate villi, but not in the terminal villi. Immature villi were present in case 3, probably because of 30 weeks of gestational age. Chorangioma was also identified in case 3. There was no villous chorangiosis, edematous change of villous stroma, or mesenchymal dysplasia characterized by grapelike vesicles in cases 1–3. Although the terminal villi exhibited no definitive abnormalities in the LM studies, EM examinations revealed swelling of vascular endothelial cells and hypertrophic change of pericytes in the terminal villi, together with narrowed capillary lumens, in cases 1 and 2.

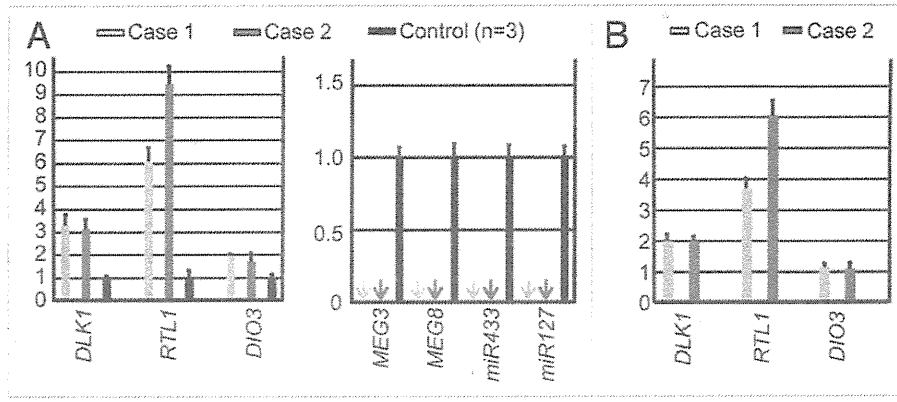

Figure 3. Quantitative real-time PCR analysis using placental samples. For a control, a pooled RNA sample consisting of an equal amount of total RNA extracted from three fresh control placentas was utilized. **(A)** Relative mRNA expression levels for *DLK1*, *RTL1*, and *DIO3* against *GAPDH* (mean ± SE) and lack of *MEGs* expression (indicated by arrows) (*miR433* and *miR127* are encoded by *RTL1as*) in the placental samples of cases 1 and 2. **(B)** Relative mRNA expression levels for *DLK1*, *RTL1*, and *DIO3* against *GAPDH* (mean ± SE), in the equal amount of expression positive placental cells (vascular endothelial cells and pericytes) of cases 1 and 2 (corrected for the difference in the relative proportion of expression positive cells between the placental samples of cases 1 and 2 and the control placental samples, on the assumption that the *DLK1* expression level is "simply doubled" in the expression positive placental cells of case 1 and 2).

IHC examinations identified RTL1, DLK1 and DIO3 protein expressions in the vascular endothelial cells and pericytes of chorionic villi, but not in the cytotrophoblasts, syncytiotrophoblasts, and stromal cells, in the placentas of cases 1–3 and in the control placenta. The PEGs protein expression level was variable in the control placenta, with moderate DLK1 expression, high RTL1 expression, and low DIO3 expression. Furthermore, DLK1 protein expression was apparently stronger in the placentas of cases 1 and 2 than in the placenta of case 3 and the control placenta, RTL1 protein expression was obviously stronger in the placentas of cases 1–3 than in the control placenta, and DIO3 protein expression was apparently similar between the placentas of cases 1–3 and the control placenta.

Discussion

We studied placental samples obtained from cases 1–3 with typical body and placental upd(14)pat phenotype. In this regard, the microsatellite data suggest that upd(14)pat with heterodisomic and isodisomic loci in case 1 was caused by trisomy rescue or gamete complementation, and that upd(14)pat with isodisomic loci alone in case 2 resulted from monosomy rescue or postzygotic mitotic error, although it is possible that heterodisomic locus/loci remained undetected in case 2.[15] Notably, there was no trace of a maternally inherited locus indicative of the presence of trisomic cells or normal cells with biparentally inherited chromosome 14 homologs in the placentas as well as in the leukocytes of cases 1 and 2. In addition, the microdeletion of case 3 has been shown to be inherited from the mother with the same microdeletion.[2] These findings imply that the placental tissues as well as the leukocytes of cases 1–3 almost exclusively, if not totally, consisted of cells with upd(14)pat or those with the microdeletion.

The q-PCR analysis was performed for the fresh placental samples of cases 1 and 2. In this context, two matters should be pointed out. First, the proportion of vascular endothelial cells and pericytes expressing *DLK1*, *RTL1*, and *DIO3* would be somewhat variable among samples, because only a small portion of the placenta was analyzed. This would be relevant to the some degree of difference in the expression levels between the placental samples of cases 1 and 2. Second, the relative proportion of vascular endothelial cells and pericytes expressing *DLK1*, *RTL1*, and *DIO3* would be higher in the placental samples of cases 1 and 2 than in the control placental samples, because the placentas of cases 1 and 2 were accompanied by proliferation of the chorionic villi with such expression positive cells. Thus, it would be inappropriate to perform a simple comparison of relative expression levels against *GAPDH* between the placental samples of cases 1 and 2 and the control placental samples. Indeed, although a complex regulatory mechanism(s), as implicated for the *RTL1* expression,[1,2] is unlikely to be operating for the *DLK1* expression, the relative *DLK1* expression level was 3.3 times and 3.1 times, not 2 times, higher in the placental samples of cases 1 and 2 than in the control placental samples, respectively (Fig. 3A). Assuming that *DLK1* expression level is simply doubled in expression positive cells of cases 1 and 2, it is predicted that the relative proportion of such expression positive cells is 1.65 times (3.3 ÷ 2.0) and 1.55 times (3.1 ÷ 2.0) larger in the placental samples of cases 1 and 2 than in the control placental samples, respectively. Thus, the expression level against *GAPDH*

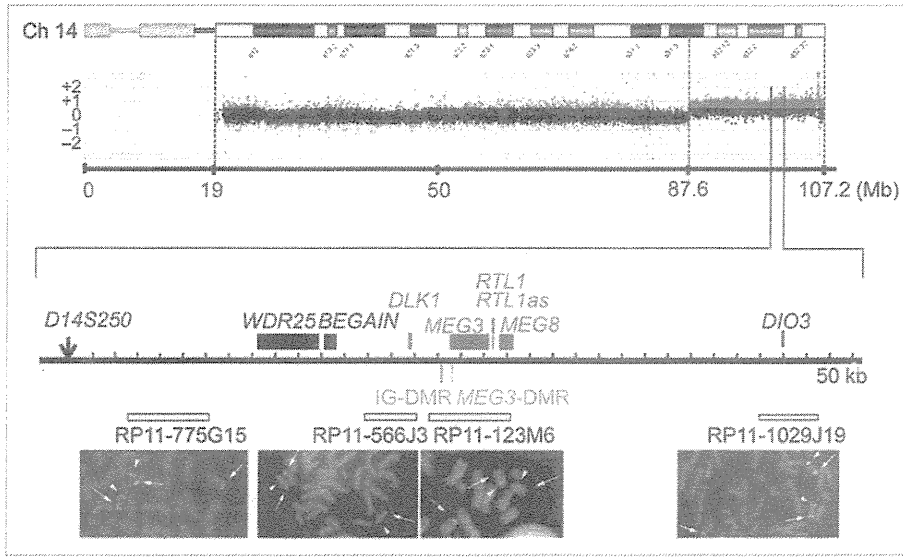

Figure 4. Array CGH and FISH analysis for the distal chromosome 14 region in case 4. In CGH analysis, the black, the red, and the green dots denote signals indicative of the normal, the increased (> +0.5), and the decreased (< −1.0) copy numbers, respectively. In FISH analysis, red signals (arrows) are derived from the probes detecting the various parts of the 14q32.2 imprinted region (the physical positions are indicated with yellow bars), and the green signals (arrowheads) are derived from an RP11-566I2 probe for 14q11.2 used as an internal control.

in the equal amount of expression positive cells is estimated as 3.69 times (6.1 ÷ 1.65) increased for *RTL1* and 1.15 times (1.9 ÷ 1.65) increased for *DIO3* in case 1, and as 6.06 times (9.4 ÷ 1.55) increased for *RTL1* and 1.09 times (1.7 ÷ 1.55) increased for *DIO3* in case 2 (**Fig. 3B**).

Thus, the expression data are summarized as follows (**Fig. 6**). First, it is inferred that the relative *RTL1* expression level is markedly (~5 times) increased in the expression positive cells of the placentas with upd(14)pat, as compared with the control placentas. This degree of elevation is grossly similar to that identified in the body of mice with the targeted deletion of the maternally derived IG-DMR (~4.5 times).[5] Such a markedly increased *RTL1* expression would be explained by assuming that *RTL1as*-encoded microRNAs (e.g., *miR433* and *miR127*) function as a repressor for *RTL1* expression through the RNAi mechanism, as has been indicated for the mouse *Rtl1-Rtl1as* interaction.[16,17] Second, it is unlikely that *DIO3* is solely expressed from the paternally inherited allele, although it remains to be determined whether *DIO3* undergoes partial imprinting like mouse *Dio3*[12] or completely escapes imprinting. In either case, the results would explain why patients with upd(14)pat and upd(14)mat lack clinically recognizable thyroid disorders,[2] although *DIO3* plays a critical role in the inactivation of thyroid hormones.[18]

This study provides further support for a critical role of excessive *RTL1* expression in the development of upd(14)pat phenotype (**Fig. 6**). Indeed, markedly (~5 times) increased *RTL1* expression is shared in common by cases 1–3 with typical upd(14)pat body and placental phenotype. In this context, it is notable that case 4 had no clinically recognizable upd(14)pat body and placental phenotype, except for omphalocele. This would imply that a single copy of *RTL1as* can almost reduce the *RTL1* expression dosage below the threshold level for the development of upd(14)pat phenotype by exerting a trans-acting repressor effect on the two functional copies of *RTL1*. By contrast, the relevance of *DLK1* to upd(14)pat phenotype is unlikely, because case 3 exhibited typical upd(14)pat phenotype in the presence of a single functional copy of *DLK1*, and case 4 showed no upd(14)pat phenotype except for omphalocele in the presence of two functional copies of *DLK1*. Similarly, if *DIO3* were more or less preferentially expressed from paternally inherited allele, the relevance of *DIO3* to upd(14)pat phenotype would also remain minor, if any. Case 4 had no upd(14)pat phenotype except for omphalocele in the presence of with two copies of *DIO3* of paternal origin. It should be pointed out, however, that the absence of *MEGs* expression may have a certain effect on the development of upd(14)pat phenotype.

The placental histological examinations revealed several informative findings. First, DLK1, RTL1, and DIO3 proteins were specifically identified in vascular endothelial cells and pericytes of chorionic villi in the control placenta, with RTL1 protein being most strongly expressed. These results, together with abnormal LM and EM findings of such cells in cases 1–3, suggest that these proteins, especially RTL1 protein, plays a pivotal role in the development of endothelial cells and pericytes. In this regard, it may be possible that the endothelial thickening and resultant narrowing the capillary lumens in the terminal villi have resulted in the dilatation of the stem to intermediate portions of the chorionic villi.

Second, the degree of protein staining was well correlated with the expression dosage of corresponding genes. In this regard, since characteristic macroscopic and microscopic placental features were identified in cases 1–3 who shared markedly elevated RTL1 protein expression, this is consistent with the notion that upd(14)pat phenotype is primarily caused by the markedly

elevated *RTL1* expression.[2] Indeed, DLK1 protein expression was not exaggerated in case 3 with typical upd(14)pat phenotype, and DIO3 protein expression was not enhanced in cases 1–3. It may be possible, however, that the abnormality of placental structures may have resulted in a difference in immunostaining without an actual change in gene expression. This point awaits further investigations.

Third, villous chorangiosis, stromal expansion, and mesenchymal dysplasia were not identified in the placental samples of cases 1–3, although such a lesion(s) may have existed in non-examined portions. Notably, such lesions are frequently observed in placentas of patients with BWS.[19-21] Thus, while both upd(14)pat and BWS are associated with placentomegaly and polyhydroamnios, characteristic histological findings appear to be different between upd(14)pat and BWS.

This study would also provide useful information on the methylation patterns of the *MEG3*-DMR in the placenta. Our previous studies using formalin-fixed and paraffin-embedded placental samples revealed that roughly two-thirds of clones were hypermethylated and the remaining roughly one-third of clones were hypomethylated in case 3 as well as in the previously reported patients with upd(14)pat (not cases 1 and 2) and epimutation (hypermethylation of the IG-DMR and the *MEG3*-DMR of maternal origin), and that roughly one-third of clones were hypermethylated and the remaining roughly two-thirds of clones were hypomethylated in control placental samples (see Fig. S2C in ref. 2). However, this study showed that the *MEG3*-DMR was grossly hypomethylated in the fresh placental samples of cases 1 and 2, with an extent similar to that identified in the fresh control placental samples. In this regard, it is notable that PCR products could be obtained only after 35 cycles for the formalin-fixed and paraffin-embedded placental samples and were sufficiently obtained after 30 cycles for the fresh placental samples. Thus, several specific clones may have been selectively amplified in the previous study. Furthermore, it may be possible that efficacy of bisulfite treatment (conversion of unmethylated cytosine into uracils and subsequently thymines) may be insufficient for the formalin-fixed and paraffin-embedded placental samples. Thus, it appears that the present data denote precise methylation patterns of the *MEG3*-DMR in the placenta.

In summary, the present study provides useful clues for the clarification of regulatory mechanism for the *RTL1* expression, imprinting status of *DIO3* and characteristic placental histological findings in patients with upd(14)pat and related conditions. Further studies will help improve our knowledge about upd(14)pat and related conditions.

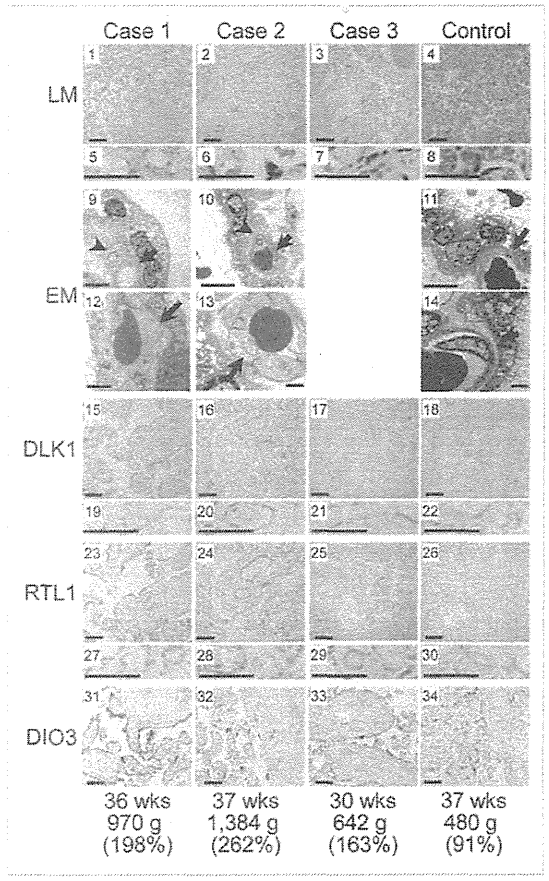

Figure 5. Histological examinations. LM, light microscopic examinations; EM, electron microscopic examinations; DLK1, RTL1 and DIO3, immunohistochemical examinations for the corresponding proteins. The arrows and arrowheads in the EM findings indicate endothelial cells and pericytes, respectively. Scale bars represent 100 μm for 1–4, 15–18, 23–26 and 31–34, 50 μm for 5–8, 19–22 and 27–30, 5 μm for 9–11 and 2 μm for 12–14. Gestational age, placental weight, and % placental weight assessed by the gestational age-matched Japanese references for placental weight[4,22] are described.

Methods

Ethical approval. This study was approved by the Institutional Review Board Committees of each investigator, and performed after obtaining written informed consent.

Primers. Primers utilized in this study are summarized in **Table S3.**

Sample preparation for molecular studies. Genomic DNA samples were obtained from leukocytes using FlexiGene DNA Kit (Qiagen) and from placental samples using ISOGEN (Nippon Gene). Transcripts of *DLK1, MEG3, RTL1, MEG8* and *DIO3* were isolated with ISOGEN (Nippon Gene), and *microRNAs* were extracted with mirVana™ miRNA Isolation Kit (Ambion). After DNase treatment, cDNA samples for *DLK1, MEG3, MEG8* and *DIO3* were prepared with oligo(dT) primers from 1 μg of RNA using Superscript III Reverse Transcriptase (Invitrogen), and those of *microRNAs* were synthesized from 300 ng of RNA using TaqMan MicroRNA Reverse Transcription Kit (Applied Biosystems). For *RTL1*, 3'-RACE was utilized to prevent amplification of *RTL1as*; cDNA was synthesized from 1 μg of RNA using Superscript III Reverse Transcriptase with a long primer hybridizing to poly A site and introducing the adaptor sequence. Lymphocyte metaphase spreads for FISH analysis were prepared from leukocytes using colcemide (Invitrogen).

Molecular studies. Microsatellite analysis for 19 loci on chromosome 14, methylation analysis for the IG-DMR and

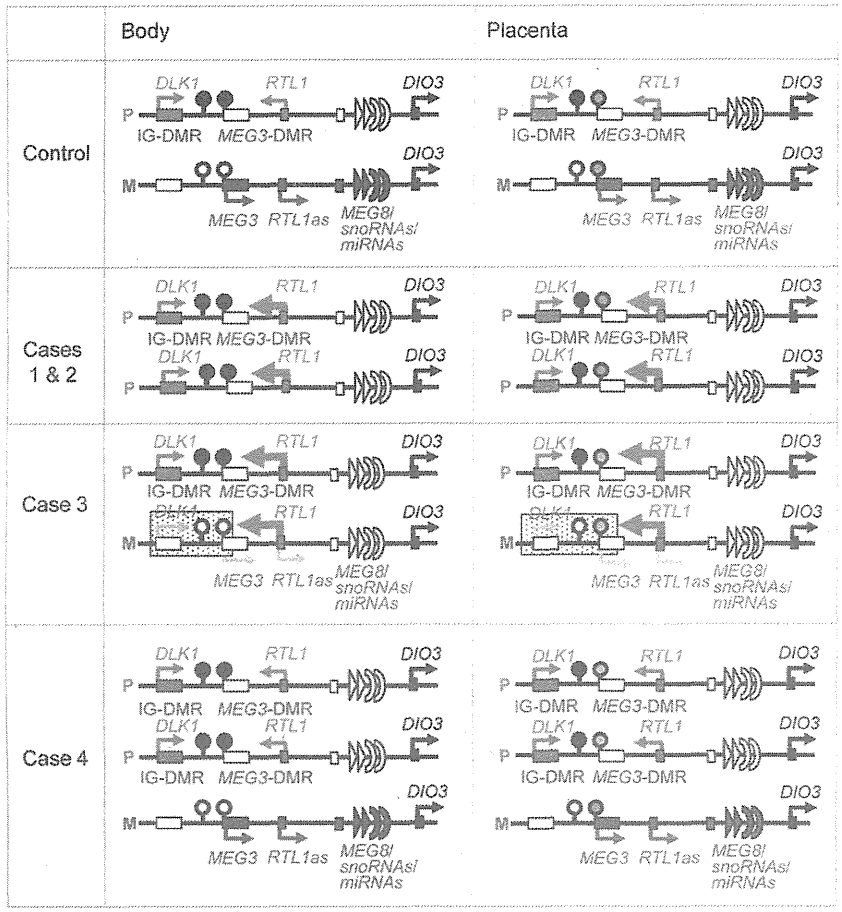

Figure 6. Schematic representation of the chromosome 14q32.2 imprinted region in a control subject, cases 1 and 2 with upd(14)pat, case 3 with a microdeletion (indicated by stippled rectangles), and case 4 with two copies of the imprinted region of paternal origin and a single copy of the imprinted region of maternal origin. This figure has been constructed using the present results and the previous data.[2,3] P, paternally derived chromosome; M, maternally derived chromosome. Filled and open circles represent hypermethylated and hypomethylated DMRs, respectively; since the *MEG3*-DMR is grossly hypomethylated and regarded as non-DMR in the placenta, it is painted in gray. *PEGs* (*DLK1* and *RTL1*) are shown in blue, *MEGs* (*MEG3*, *RTL1as*, *MEG8*, *snoRNAs* and *miRNAs*) in red, a probably non-imprinted gene (*DIO3*) in black, and non-expressed genes in white. Thick arrows for *RTL1* in cases 1–3 represent increased *RTL1* expression that is ascribed to loss of functional microRNA-containing *RTL1as* as a repressor for *RTL1*.

the *MEG3*-DMR, and FISH analyses for the 14q32.2 region were performed as described previously.[2,3] For FISH analysis of 17p13.3, a 17p sub-telomere probe and an RP11–411G7 probe for the 17p13.3 region were utilized, together with a CEP17 probe for the 17p11.1 region utilized as an internal control. The 17p sub-telomere probe was detected according to the manufacture's protocol, the RP11–411G7 probe was labeled with digoxigenin and detected by rhodamine anti-digoxigenin, and the CEP17 control probe was labeled with biotin and detected by avidin conjugated to fluorescein isothiocyanate. Quantitative real-time PCR analysis was performed on an ABI PRISM 7000 (Applied Biosystems) using TaqMan real-time PCR probe primer mixture for the following genes (assay No: Hs00171584 for *DLK1*, Hs00292028 for *MEG3*, Hs00419701 for *MEG8* and Hs00704811 for *DIO3*; assay ID: 001028 for *miR433* and 000452 for *miR127*). For *RTL1*, q-PCR analysis was performed with a forward primer hybridized to the sequence of *RTL1* and a reverse primer hybridized to the adaptor sequence. Fifty nanongrams of cDNA in a 50 μl reaction mixture contacting 2× KOD FX buffer (Toyobo), 2.0 mM dNTP mixture (Toyobo), KOD FX (Toyobo), SYBR Green I (Invitrogen), and primer set for *RTL1* were subjected to the ABI PRISM 7000. Data were normalized against *GAPDH* (catalog No: 4326317E) for *DLK1*, *MEG3*, *MEG8*, *RTL1*, and *DIO3*, and against *RNU48* (assay ID: 0010006) for *microRNAs*. The expression studies were performed three times for each sample. Oligoarray CGH was performed using 1× 1M format Human Genome Array (Catalog No G4447A) (Agilent Technologies).

Histopathogical analysis. Placental samples were fixed with 20% buffered formaldehyde at room temperature and embedded in paraffin wax according to standard protocols for LM examinations. Then, sections of 3 μm thick were stained with hematoxylin-eosin. For EM examinations, fresh placental tissues were fixed with phosphate-buffered 2.5% glutaraldehyde, postfixed in 1% osmium tetroxide, and embedded in Epon 812 (catalog No. R3245, TAAB). Semithin sections were stained with 1% methylene blue, and ultrathin sections were double-stained with uranyl acetate and lead citrate. Subsequently, they were examined with a Ninhon Denshi JEM-1230 electron microscope.

For IHC analysis, sections of 3 μm thick were prepared by the same methods utilized for the LM examinations, and were examined with rabbit anti human DLK1 polyclonal antibody at 1:100 dilutions (catalog No 10636-1-AP, ProteinTech Group), rabbit anti human RTL1 polyclonal antibody at 1:200 dilutions, and rabbit anti human DIO3 polyclonal antibody at 1:50 dilutions (catalog No ab102926, abcam); anti human RTL1 polyclonal antibody was produced by immunizing rabbits with the synthesized RTL1 peptide (NH2-RGFPRDPSTESG-COOH) in this study. Sections were dewaxed in xylene and rehydrated through graded ethanol series and, subsequently, incubated in 10% citrate buffer (pH 6.0) for 40 min in a 98°C water bath, for antigen retrieval. Endogenous peroxidase activity was quenched with 1% H_2O_2 and 100% methanol for 20 min. To prevent non-specific background staining, sections are incubated with Protein Block Serum-Free (Dako corporation) for 10 min at room temperature. Then, sections were incubated overnight with primary antibody at 4°C

and, subsequently, treated with the labeled polymer prepared by combining amino acid polymers with peroxidase and anti-rabbit polyclonal antibody (Histofine Simple Stain MAX PO MULTI, Nichirei). Peroxidase activities were visualized by diaminobenzidine staining, and the nuclei were stained with hematoxylin.

Disclosure of Potential Conflicts of Interest

No potential conflicts of interest were disclosed.

Acknowledgments

This work was supported by Grants-in-Aid for Scientific Research (A) (22249010) and Research (B) (21028026) from the Japan Society for the Promotion of Science (JSPS), by Grants-in-Aid for Scientific Research on Innovative Areas (22132004-A04) from the Ministry of Education, Culture, Sports, Science and Technology (MEXT), by Grants for Research on Intractable Diseases (H22–161) from the Ministry of Health, Labor and Welfare (MHLW), by Grant for National Center for Child Health and Development (23A-1), and by Grant from Takeda Science Foundation and from Novartis Foundation.

Supplemental Materials

Supplemental materials may be found here:
www.landesbioscience.com/journals/epigenetics/article/21937

References

1. da Rocha ST, Edwards CA, Ito M, Ogata T, Ferguson-Smith AC. Genomic imprinting at the mammalian Dlk1-Dio3 domain. Trends Genet 2008; 24:306-16; PMID:18471925; http://dx.doi.org/10.1016/j.tig.2008.03.011.
2. Kagami M, Sekita Y, Nishimura G, Irie M, Kato F, Okada M, et al. Deletions and epimutations affecting the human 14q32.2 imprinted region in individuals with paternal and maternal upd(14)-like phenotypes. Nat Genet 2008; 40:237-42; PMID:18176563; http://dx.doi.org/10.1038/ng.2007.56.
3. Kagami M, O'Sullivan MJ, Green AJ, Watabe Y, Arisaka O, Masawa N, et al. The IG-DMR and the MEG3-DMR at human chromosome 14q32.2: hierarchical interaction and distinct functional properties as imprinting control centers. PLoS Genet 2010; 6:e1000992; PMID:20585555; http://dx.doi.org/10.1371/journal.pgen.1000992.
4. Kagami M, Yamazawa K, Matsubara K, Matsuo N, Ogata T. Placentomegaly in paternal uniparental disomy for human chromosome 14. Placenta 2008; 29:760-1; PMID:18619672; http://dx.doi.org/10.1016/j.placenta.2008.06.001.
5. Lin SP, Youngson N, Takada S, Seitz H, Reik W, Paulsen M, et al. Asymmetric regulation of imprinting on the maternal and paternal chromosomes at the Dlk1-Gtl2 imprinted cluster on mouse chromosome 12. Nat Genet 2003; 35:97-102; PMID:12937418; http://dx.doi.org/10.1038/ng1233.
6. Sekita Y, Wagatsuma H, Nakamura K, Ono R, Kagami M, Wakisaka N, et al. Role of retrotransposon-derived imprinted gene, Rtl1, in the feto-maternal interface of mouse placenta. Nat Genet 2008; 40:243-8; PMID:18176565; http://dx.doi.org/10.1038/ng.2007.51.
7. Lage JM. Placentomegaly with massive hydrops of placental stem villi, diploid DNA content, and fetal omphaloceles: possible association with Beckwith-Wiedemann syndrome. Hum Pathol 1991; 22:591-7; PMID:1864589; http://dx.doi.org/10.1016/0046-8177(91)90237-J.
8. Yamazawa K, Kagami M, Nagai T, Kondoh T, Onigata K, Maeyama K, et al. Molecular and clinical findings and their correlations in Silver-Russell syndrome: implications for a positive role of IGF2 in growth determination and differential imprinting regulation of the IGF2-H19 domain in bodies and placentas. J Mol Med (Berl) 2008; 86:1171-81; PMID:18607558; http://dx.doi.org/10.1007/s00109-008-0377-4.
9. Georgiades P, Watkins M, Burton GJ, Ferguson-Smith AC. Roles for genomic imprinting and the zygotic genome in placental development. Proc Natl Acad Sci U S A 2001; 98:4522-7; PMID:11274372; http://dx.doi.org/10.1073/pnas.081540898.
10. Fowden AL, Sibley C, Reik W, Constancia M. Imprinted genes, placental development and fetal growth. Horm Res 2006; 65(Suppl 3):50-8; PMID:16612114; http://dx.doi.org/10.1159/000091506.
11. Georgiades P, Ferguson-Smith AC, Burton GJ. Comparative developmental anatomy of the murine and human definitive placentae. Placenta 2002; 23:3-19; PMID:11869088; http://dx.doi.org/10.1053/plac.2001.0738.
12. Tsai CE, Lin SP, Ito M, Takagi N, Takada S, Ferguson-Smith AC. Genomic imprinting contributes to thyroid hormone metabolism in the mouse embryo. Curr Biol 2002; 12:1221-6; PMID:12176332; http://dx.doi.org/10.1016/S0960-9822(02)00951-X.
13. Yamanaka M, Ishikawa H, Saito K, Maruyama Y, Ozawa K, Shibasaki J, et al. Prenatal findings of paternal uniparental disomy 14: report of four patients. Am J Med Genet A 2010; 152A:789-91; PMID:20186803; http://dx.doi.org/10.1002/ajmg.a.33247.
14. Suzumori N, Ogata T, Mizutani E, Hattori Y, Matsubara K, Kagami M, et al. Prenatal findings of paternal uniparental disomy 14: Delineation of further patient. Am J Med Genet A 2010; 152A:3189-92; PMID:21108407; http://dx.doi.org/10.1002/ajmg.a.33719.
15. Kagami M, Kato F, Matsubara K, Sato T, Nishimura G, Ogata T. Relative frequency of underlying genetic causes for the development of UPD(14)pat-like phenotype. Eur J Hum Genet 2012; 20:928-32; PMID:22353941; http://dx.doi.org/10.1038/ejhg.2012.26.
16. Seitz H, Youngson N, Lin SP, Dalbert S, Paulsen M, Bachellerie JP, et al. Imprinted microRNA genes transcribed antisense to a reciprocally imprinted retrotransposon-like gene. Nat Genet 2003; 34:261-2; PMID:12796779; http://dx.doi.org/10.1038/ng1171.
17. Davis E, Caiment F, Tordoir X, Cavaillé J, Ferguson-Smith A, Cockett N, et al. RNAi-mediated allelic trans-interaction at the imprinted Rtl1/Peg11 locus. Curr Biol 2005; 15:743-9; PMID:15854907; http://dx.doi.org/10.1016/j.cub.2005.02.060.
18. Köhrle J. Thyroid hormone transporters in health and disease: advances in thyroid hormone deiodination. Best Pract Res Clin Endocrinol Metab 2007; 21:173-91; PMID:17574002; http://dx.doi.org/10.1016/j.beem.2007.04.001.
19. Kraus FT, Redline RW, Gersell DJ, Nelson DM, Dicker JM. Disorders of placental Development. Placental Pathology (Atlas of Noutumor Pathology). Washington, DC: American Registry of Pathology, 2004:59-68.
20. Fox HE, Sebire NJ. The placenta in abnormalities and disorders of the fetus. Pathology of the Placenta. Third edition, Philadelphia, PA: SAUNDERS, 2007:262-3.
21. Parveen Z, Tongson-Ignacio JE, Fraser CR, Killeen JL, Thompson KS. Placental mesenchymal dysplasia. Arch Pathol Lab Med 2007; 131:131-7; PMID:17227114.
22. Nakayama M. Placental pathology. Tokyo, Igaku Shoin, 2002:106-7 (in Japanese).

Mamld1 Deficiency Significantly Reduces mRNA Expression Levels of Multiple Genes Expressed in Mouse Fetal Leydig Cells but Permits Normal Genital and Reproductive Development

Mami Miyado, Michiko Nakamura, Kenji Miyado, Ken-ichirou Morohashi, Shinichiro Sano, Eiko Nagata, Maki Fukami, and Tsutomu Ogata

Departments of Molecular Endocrinology (M.M., M.N., M.F., T.O.) and Reproductive Biology (K.Mi.), National Research Institute of Child Health and Development, Tokyo 157-8535, Japan; Department of Molecular Biology (K.Mo.), Graduate School of Medical Sciences, Kyushu University, Fukuoka 812-8582, Japan; and Department of Pediatrics (S.S., E.N., T.O.), Hamamatsu University School of Medicine, Hamamatsu 431-3192, Japan

Although mastermind-like domain containing 1 (*MAMLD1*) (*CXORF6*) on human chromosome Xq28 has been shown to be a causative gene for 46,XY disorders of sex development with hypospadias, the biological function of *MAMLD1*/*Mamld1* remains to be elucidated. In this study, we first showed gradual and steady increase of testicular *Mamld1* mRNA expression levels in wild-type male mice from 12.5 to 18.5 d postcoitum. We then generated *Mamld1* knockout (KO) male mice and revealed mildly but significantly reduced testicular mRNA levels (65–80%) of genes exclusively expressed in Leydig cells (*Star*, *Cyp11a1*, *Cyp17a1*, *Hsd3b1*, and *Insl3*) as well as grossly normal testicular mRNA levels of genes expressed in other cell types or in Leydig and other cell types. However, no demonstrable abnormality was identified for cytochrome P450 17A1 and 3β-hydroxysteroid dehydrogenase (HSD3B) protein expression levels, appearance of external and internal genitalia, anogenital distance, testis weight, Leydig cell number, intratesticular testosterone and other steroid metabolite concentrations, histological findings, *in situ* hybridization findings for *sonic hedgehog* (the key molecule for genital tubercle development), and immunohistochemical findings for anti-Müllerian hormone (Sertoli cell marker), HSD3B (Leydig cell marker), and DEAD (Asp-Glu-Ala-Asp) box polypeptide 4 (germ cell marker) in the KO male mice. Fertility was also normal. These findings imply that *Mamld1* deficiency significantly reduces mRNA expression levels of multiple genes expressed in mouse fetal Leydig cells but permits normal genital and reproductive development. The contrastive phenotypic findings between *Mamld1* KO male mice and *MAMLD1* mutation positive patients would primarily be ascribed to species difference in the fetal sex development. **(*Endocrinology* 153: 6033–6040, 2012)**

Mastermind-like domain containing 1 (*MAMLD1*) (alias *CXORF6*) on human chromosome Xq28 is a causative gene for 46,XY disorders of sex development (DSDs) with hypospadias as a salient clinical phenotype. Indeed, several pathologic nonsense and frameshift mutations (p.E124X, p.Q197X, p.R653X, and p.E109fsX121) have been identified in patients with various types of hypospadias with and without other associated genital abnormalities, such as micropenis and cryptorchidism (1–3). In addition, a specific polymorphism(s) and a haplotype of *MAMLD1* appear to constitute a genetic risk factor for hypospadias (2, 4, 5).

To date, several important findings have been revealed for *MAMLD1* and its mouse homolog *Mamld1*. First, the

ISSN Print 0013-7227 ISSN Online 1945-7170
Printed in U.S.A.

doi: 10.1210/en.2012-1324 Received March 21, 2012. Accepted September 20, 2012.
First Published Online October 18, 2012

Abbreviations: Ab, Antibody; AGD, anogenital distance; AGI, AGD index; CYP17A1, cytochrome P450 17A1; dpc, days postcoitum; DSD, disorder of sex development; HSD3B, 3β-hydroxysteroid dehydrogenase; KO, knockout; *MAMLD1*, mastermind-like domain containing 1; MLTC, mouse Leydig tumor cell; *Shh*, *sonic hedgehog*; siRNA, small interfering RNA; T, testosterone; WT, wild type.

upstream region of *MAMLD1/Mamld1* harbors a putative binding site for *NR5A1* (alias *SF-1* and *AD4BP*) (6) that regulates the transcription of a vast array of genes involved in sex development (7). Second, nuclear receptor subfamily 5, group A, member 1 protein can bind to the putative target site and exert a transactivation function for *Mamld1* (6). Third, *Mamld1* is clearly coexpressed with mouse *Nr5a1* in fetal Leydig and Sertoli cells in the fetal testis (1). Fourth, transient *Mamld1* knockdown using small interfering RNAs (siRNAs) significantly reduces *Cyp17a1* expression (8) and testosterone (T) production in cultured mouse Leydig tumor cells (MLTCs) (6, 8). These findings imply that *MAMLD1/Mamld1* is involved in the molecular network for T production probably via the transactivation of *CYP17A1/Cyp17a1* under the regulation of *NR5A1* and that *MAMLD1* mutations result in 46,XY DSD phenotype with hypospadias primarily because of compromised, but not abolished, T production around the critical period for sex development.

However, the biological function of *MAMLD1/Mamld1* during testis development remains to be elucidated. Thus, we examined testicular *Mamld1* mRNA expression pattern in wild-type (WT) male mice and performed molecular and phenotypic analyses in *Mamld1* knockout (KO) male mice.

Materials and Methods

WT and *Mamld1* KO male mice

We examined WT male mice of the C57BL/6 strain purchased from Sankyo Labo Service Corp., Inc. (Tokyo, Japan) and *Mamld1* KO male mice generated by Macrogen, Inc. (Seoul, Korea). This study was approved by the Animal Ethics Committee of National Research Institute for Child Health and Development.

Mamld1 KO male mice were produced by a standard gene-targeting procedure (9). In brief, a targeting vector was designed to replace *Mamld1* exon 3, which harbors a translation start codon and approximately two thirds of the coding sequence, with a *PGK-neo* cassette (Fig. 1A). After transfection of the targeting vector into 129/Sv embryonic stem cells by electroporation, two clones of recombination-positive embryonic stem cells were selected by Southern blot analysis using probes at the 5′ and 3′ flanking regions of *Mamld1* and injected into blastocysts. The blastocysts were then transferred into pseudopregnant ICR female mice, to generate chimeric male mice. The chimeric male mice were mated with C57BL/6 female mice, and germline transmission of the mutant gene was confirmed by Southern blot analysis. Subsequently, *Mamld1* KO male mice were produced by mating heterozygous (+/−) female mice with WT male mice. The *Mamld1* KO mouse strain was backcrossed with the C57BL/6 strain and maintained for multiple generations by cross-mating between heterozygous (+/−) female mice and WT male mice.

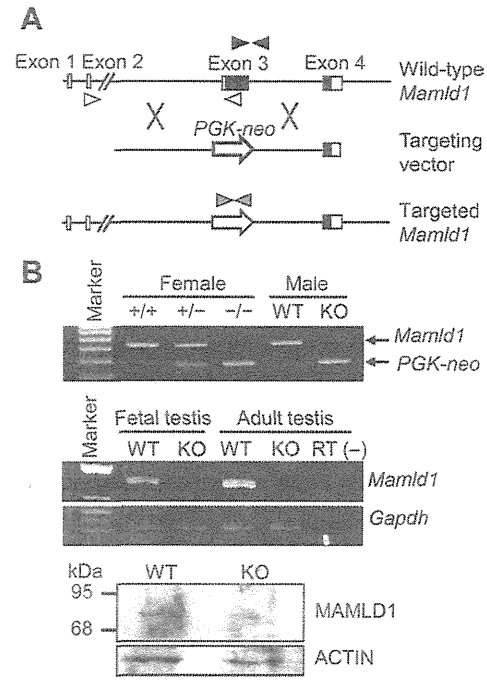

FIG. 1. Generation of *Mamld1* KO mice. A, Schematic representation of the gene targeting procedure. Exon 3 of WT *Mamld1* was replaced by the *PGK-neo* cassette (*PGK-neo*) through homologous recombination indicated by *cross symbols*. The *black and white boxes* denote the coding regions and the untranslated regions, respectively. *Paired black, white, and gray arrowheads* indicate the primer set for amplification of WT *Mamld1* genomic sequence, that for amplification of *Mamld1* transcripts, and that for amplification of Neomycin-resistant gene. B, Confirmation of *Mamld1* KO. Genotyping analysis (*upper panel*), RT-PCR analysis (*middle panel*), and Western blot analysis (*lower panel*) are consistent with successful *Mamld1* KO. +/+, WT female mice; +/−, heterozygous female mice; −/−, homozygous female mice; RT (−), negative control without reverse transcriptase.

In this study, KO male mice of the ninth generation were examined. The noon of the day when a vaginal plug was observed was designated 0.5 d postcoitum (dpc). PCR-based genotyping analysis with tail tissue genomic DNA was performed for *Mamld1*, *PGK-neo*, and *Sry*, using primers shown in Supplemental Table 1, published on The Endocrine Society's Journals Online web site at http://endo.endojournals.org. Body weight and testis weight were measured at birth.

Genital and testicular sample preparation

In the male mice, androgen synthesis starts after approximately 13.5 dpc (10, 11), and morphological characteristics of the male external genitalia are established around 16.5 dpc (12, 13). Thus, genital and testicular samples were prepared from genotype- and embryonic day-matched KO male mice and their WT littermates in the latter half of the fetal life and at birth.

Real-time RT-PCR analyses

Testes from three mice were pooled in a single tube, and five tubes were prepared for each embryonic day. Total RNA was extracted from homogenized samples using ISOGEN (Nippongene, Tokyo, Japan), and cDNA was synthesized from 200 ng of total RNA using High Capacity cDNA Reverse Transcription kit (Life Technologies, Carlsbad, CA). Real-time RT-PCR was per-

formed for *Mamld1* and 17 genes involved in sex development and expressed in the fetal testis (*Amh*, *Ar*, *Arx*, *Cyp11a1*, *Cyp17a1*, *Ddx4*, *Dhh*, *Dlx5*, *Dlx6*, *Gata4*, *Hsd17b3*, *Hsd3b1*, *Insl3*, *Nr5a1*, *Ptch1*, *Sox9*, and *Star*) as well as *Gapdh* used as an internal control, using the ABI 7500 Fast real-time PCR system (Life Technologies) and TaqMan gene expression assay kit. Primers and probes used are shown in Supplemental Table 2.

Western blot analysis

Testes collected as described above were homogenized, diluted in Laemmli buffer, and heated at 95 C. Protein extracts were subjected to a standard SDS-PAGE (12% gel) and were hybridized with anti-MAMLD1-antibody (Ab), anti-cytochrome P450 17A1(CYP17A1)-Ab, and anti-3β-hydroxysteroid dehydrogenase (HSD3B)-Ab, as well as anti-ACTIN-Ab (A2066; Sigma, St. Louis, MO) used as an internal control. Anti-MAMLD1-Ab was generated against mouse MAMLD1 peptide (CGSESFLPGSSFAHE) using rabbits, anti-CYP17A1-Ab was purchased from Santa Cruz Biotechnology, Inc. (sc-46081; Santa Cruz, CA), and anti-HSD3B-Ab was as reported previously (14). Chemiluminescence signals were detected using ECL Plus Western Blot Detection kit (GE Healthcare UK Ltd., Buckinghamshire, UK), and signal densities were assessed using an Odyssey Infrared Imaging System (LI-COR Biosciences, Lincoln, NE).

Stereoscopic observation

Morphological findings of external and internal genital regions were examined, as were anogenital distance (AGD) (the distance between the anus and the penoscrotal junction) and AGD index (AGI) (AGD divided by body weight) as indicators for the androgen action during the embryonic period (15–17). Furthermore, whole mount *in situ* hybridization was performed for *sonic hedgehog* (*Shh*), one of the key molecules for the development of genital tubercle (18, 19), using an antisense cRNA fragment as a probe (GenBank accession no. BC063087; nucleotide position, 138-1499). Sense cRNA was used as a negative control. Hybridization was performed using the Wilkinson procedure (20), and signals were visualized with the BM Purple AP Substrate (Roche, Mannheim, Germany).

Histological and immunohistochemical examinations

Histological examination was performed for tissue samples that were fixed with 4% paraformaldehyde, dehydrated, and embedded in paraffin. Serial 6-μm sections were mounted on Superfrost slides, and every tenth section was stained with hematoxylin-eosin.

Immunohistochemical examination was carried out for the remaining section slides that were deparaffinized and incubated with 3% H_2O_2 in PBS to inactivate endogenous peroxidases. The slides were then incubated in blocking solution (Roche) and transferred into a new solution containing polyclonal primary Abs against anti-Mülerian hormone (sc-46081; Santa Cruz Biotechnology, Inc.) as a marker for Sertoli cells, HSD3B as a marker for Leydig cells, DEAD (Asp-Glu-Ala-Asp) box polypeptide 4 (ab13840; Abcam, Cambridge, UK) as a marker for germ cells, and proliferating cell nuclear antigen (PC10; Dako, Glostrup, Denmark) as a marker for proliferating cells. The samples were washed and incubated with secondary Abs conjugated with horseradish peroxidase (Santa Cruz Biotechnology, Inc.). The Simple Stain DAB Solution (Nichirei, Tokyo, Japan) was used for color development. Apoptotic cells were detected by terminal deoxynucleotidyl transferase 2′-deoxyuridine, 5′-triphosphate nick end labeling staining using an *In Situ* Apoptosis Detection kit (TaKaRa Bio, Shiga, Japan). Furthermore, HSD3B-positive cells in four randomly selected fields of each testis were counted, to estimate the number of Leydig cells.

Measurement of intratesticular T and steroid metabolites

Intratesticular T and steroid metabolites were measured at 18.5 dpc by liquid chromatography tandem mass spectrometry (ASKA Pharma Medical, Kanagawa, Japan) using samples stored at −80 C, because intratesticular T usually peaks at 18.5 dpc in normal mice (10, 11).

Cross-mating experiments

Cross-mating was performed between *Mamld1* KO male mice and WT or heterozygous (+/−) female mice and between WT male mice and WT or heterozygous (+/−) female mice.

Statistical analysis

The data are expressed as the mean ± SEM. Statistical significance of the mean between two groups was examined by Student's *t* test, and that of the frequency between two groups was examined by χ^2 test. $P < 0.05$ was considered significant.

Results

Mamld1 expression in the fetal testis of WT male mice

Real-time RT-PCR analyses indicated a gradual and steady increase in the *Mamld1* mRNA levels from 12.5 to 18.5 dpc (Fig. 2).

Generation of *Mamld1* KO male mice

Mamld1 KO male mouse was successfully produced. *Mamld1* exon 3 was deleted from the genome of the KO

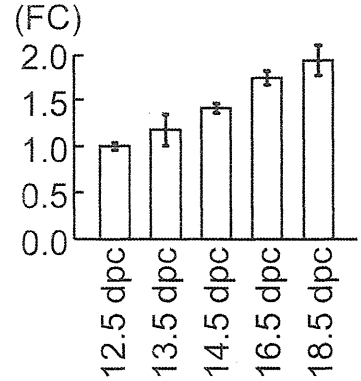

FIG. 2. Testicular *Mamld1* expression levels during the latter half of the fetal life in WT male mice. Figure indicates the data obtained by real-time RT-PCR analyses. Fold change (FC) represents relative mRNA levels of *Mamld1* against *Gapdh*. The relative expression level of *Mamld1* mRNA at 12.5 dpc was designated as 1.0.

TABLE 1. Comparison between *Mamld1* KO mice and their WT littermates

	KO	WT	*P* value
Body weight (g) (at birth)	1.48 ± 0.03 (n = 10)	1.44 ± 0.03 (n = 10)	0.40
AGD (mm) (at birth)	1.33 ± 0.02 (n = 10)	1.32 ± 0.02 (n = 10)	0.62
AGI (mm/g) (at birth)	0.90 ± 0.02 (n = 10)	0.92 ± 0.02 (n = 10)	0.55
Leydig cells (HSD3B-stained cells) (number/HPF) (at 14.5 dpc)	69.3 ± 8.2 (n = 3)	75.1 ± 7.6 (n = 3)	0.63
Testis weight (mg) (at birth)	1.46 ± 0.08 (n = 10)	1.35 ± 0.08 (n = 10)	0.34
Intratesticular steroid metabolites (at 18.5 dpc)			
Pregnenolone (pg/two testes)	17.9 ± 4.0 (n = 4)	15.4 ± 1.4 (n = 4)	0.57
Progesterone (pg/two testes)	16.5 ± 4.6 (n = 4)	15.0 ± 1.7 (n = 4)	0.56
17-OH pregnenolone (pg/two testes)	15.2 ± 2.9 (n = 4)	15.4 ± 1.3 (n = 4)	0.77
17-OH progesterone (pg/two testes)	10.4 ± 1.7 (n = 4)	13.5 ± 2.5 (n = 4)	0.15
Androstenedione (ng/two testes)	0.44 ± 0.15 (n = 4)	0.51 ± 0.07 (n = 4)	0.25
T (ng/two testes)	2.31 ± 0.30 (n = 4)	2.38 ± 0.31 (n = 4)	0.89

Expressed as mean ± SEM. HPF, High power field (234.1 × 175.5 μm).

mice, and neither *Mamld1* mRNA nor MAMLD1 protein was identified in the testis of the KO mice (Fig. 1B). Body weight was comparable between the KO male mice and their WT littermates (Table 1).

Gene and protein expression pattern in the fetal testes of *Mamld1* KO mice

The results are shown in Fig. 3. Relative mRNA levels of *Cyp17a1*, *Hsd3b1*, and *Insl3* mRNAs were mildly but

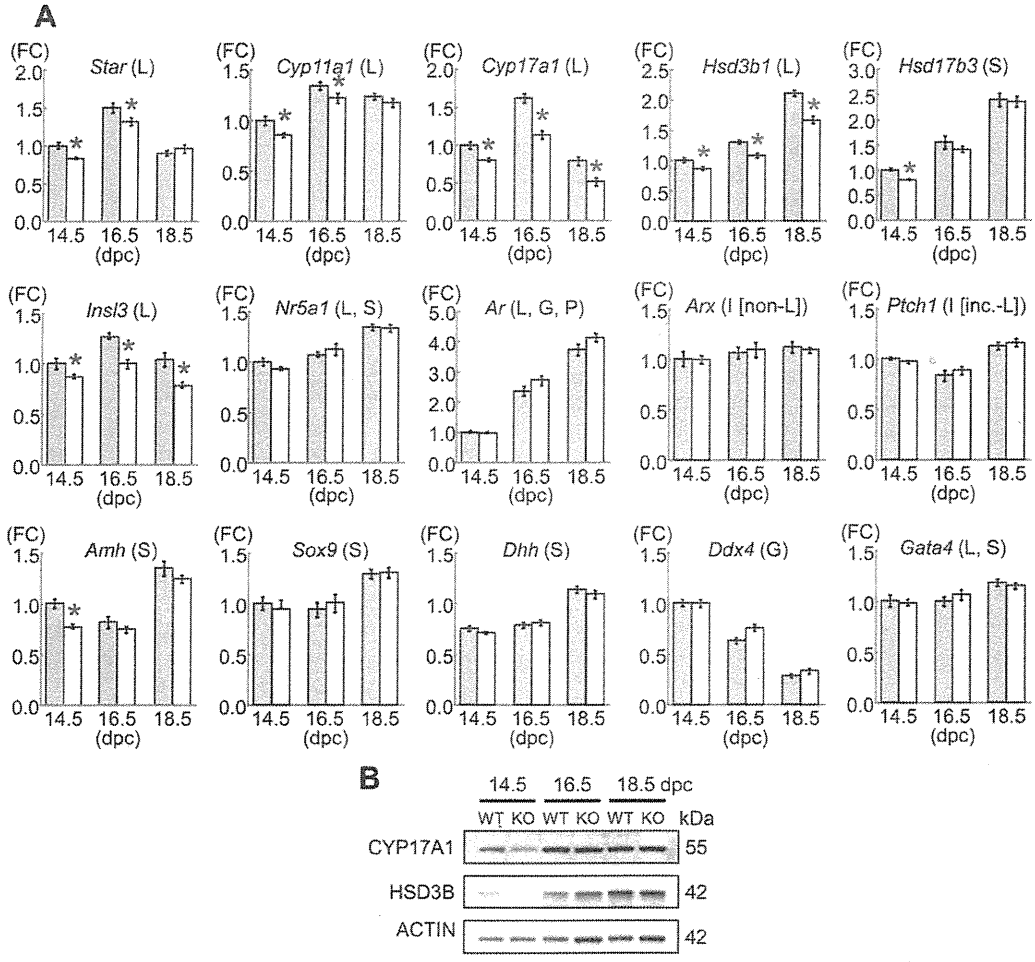

FIG. 3. Gene and protein expression patterns in the fetal testes. A, Relative mRNA levels of examined genes against *Gapdh*. FC, Fold change; L, Leydig cells; S, Sertoli cells; G, germ cells; P, peritubular cells; I [non-L], interstitial cells excluding Leydig cells; I [inc.-L], interstitial cells including Leydig cells. The *green and the yellow bars* indicate the data obtained from WT male mice and *Mamld1* KO male, respectively. For each gene, the relative expression level of mRNA in WT male mice at 14.5 dpc was designated as 1.0. *Red asterisks* indicate significant results ($P < 0.05$). B, Western blot analysis for CYP17A1 and HSD3B, as well as for ACTIN.

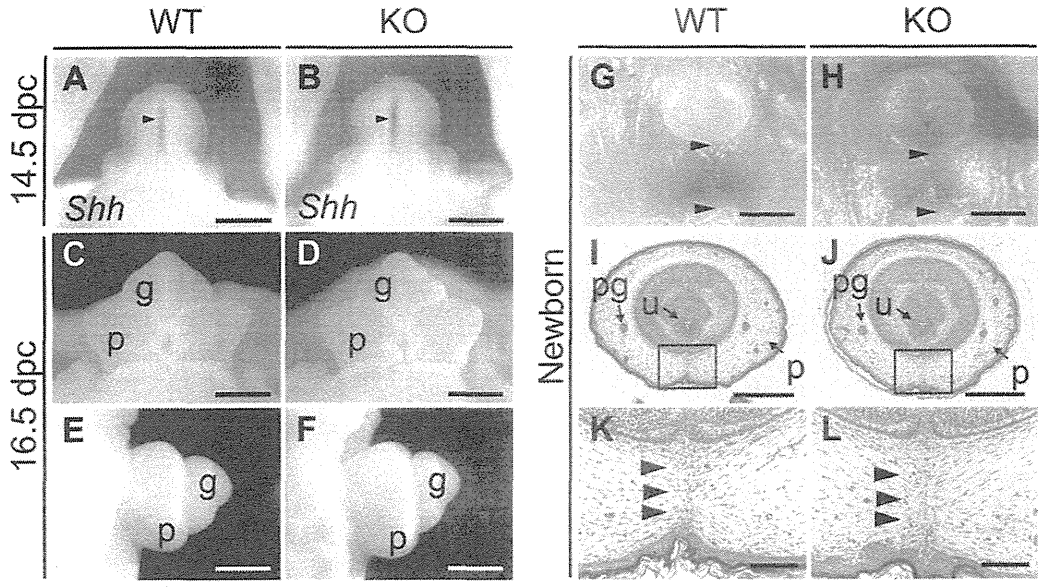

FIG. 4. External genitalia of WT and *Mamld1* KO male mice. A and B, Whole mount *in situ* hybridization for *Shh* (*arrowheads*) in the developing genital region at 14.5 dpc. C–F, Appearance of the genital tubercle at 16.5 dpc. G and H, Appearance of the external genitalia at birth. The distance between the anus and the penoscrotal junction (*arrowheads*) represents the AGD. I–L, Histological findings of the external genitalia at birth. *Arrowheads* in K and L indicate the fused prepuce. g, Glans; p, prepuce; pg, preputal gland; u, urethra. *Scale bars*: 500 μm (A–F, I, and J), 1 mm (G and H), and 100 μm (K and L).

significantly lower in the KO male mice than in their WT littermates at 14.5, 16.5, and 18.5 dpc, as were those for *Star* and *Cyp11a1* at 14.5 and 16.5 dpc (65–80%) (*Dlx5* and *Dlx6* expression levels were extremely low). By contrast, relative mRNA levels of the remaining genes were comparable between the KO male mice and their WT littermates, except for relative mRNA levels of *Hsd17b3* and *Amh* at 14.5 dpc. However, expression levels of CYP17A1 and HSD3B proteins were similar between the KO male mice and their WT littermates and were obviously higher at 16.5 and 18.5 dpc than at 14.5 dpc.

External genital findings of *Mamld1* KO male mice

External genitalia were obviously normal in the *Mamld1* KO male mice (Fig. 4 and Table 1). *Shh* was normally expressed in the urethral epithelium of the KO male mice at 14.5 dpc, and subsequent outgrowth of genital tubercle and fusion of the urethral folds at the ventral midline occurred in the KO male mice at the same embryonic stages as in their WT littermates. Furthermore, external genitalia were normally developed at birth, with the comparable AGD and AGI between the KO mice and their WT littermates.

Internal genital findings of *Mamld1* KO mice

Internal genitalia of the *Mamld1* KO male mice were also free from demonstrable abnormality (Fig. 5 and Table 1). Intraabdominal testicular descent, wolffian development, and müllerian regression were normally observed in the KO male mice at 16.5 dpc. Testicular histological findings were comparable between the KO mice and their WT littermates at 14.5 dpc and at birth. Immunohistochemical findings indicated the presence of similar numbers of Sertoli cells (anti-Müllerian hormone-stained cells), Leydig cells (HSD3B-stained cells), and germ cells [DEAD (Asp-Glu-Ala-Asp) box polyoeotide 4-stained cells] at 14.5 dpc as well as the presence of a similar number of Leydig cells (HSD3B-stained cells) at birth between the KO mice and their WT littermates. A relatively large number of mitotic cells (proliferating cell nuclear antigen-stained cells) was also identified in both the KO mice and their WT littermates, as were a small number of apoptotic cells (terminal deoxynucleotidyl transferase 2′-deoxyuridine, 5′-triphosphate nick end labeling-stained cells) (data not shown). In addition, testis weights at birth and intratesticular concentrations of T and other steroid metabolites at 18.5 dpc were also similar between the KO mice and their WT littermates.

Cross-mating experiments

The results are shown in Table 2. *Mamld1* KO male mice produced offspring with WT and heterozygous (+/−) female mice, as did WT male mice. Furthermore, the frequency of littermate offspring [*Mamld1* KO male mice, WT male mice, homozygous (−/−) female mice, heterozygous (+/−) female mice, and WT female mice] was in agreement with the expected Mendelian mode of inheritance.

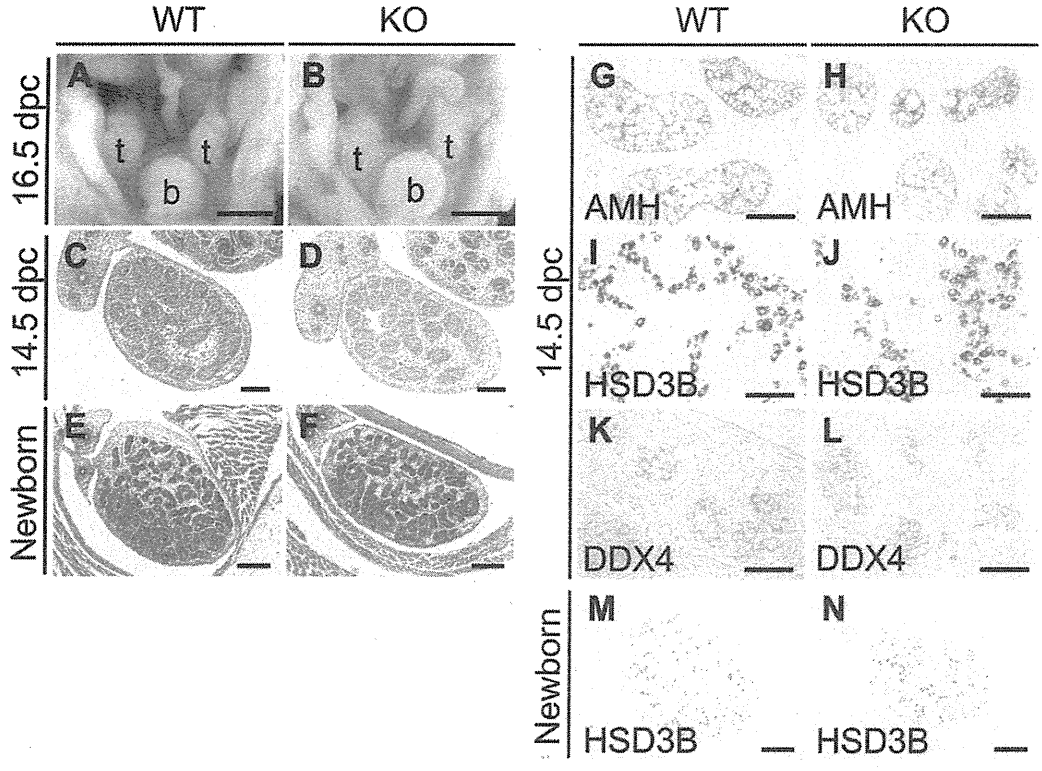

FIG. 5. Internal genitalia of WT and *Mamld1* KO male mice. A and B, Appearance of internal genital organs at 16.5 dpc. C–F, Histological findings of testes at 14.5 dpc and birth. G–N, Immunohistochemical findings of testes at 14.5 dpc and birth. b, Bladder; t, testis. *Scale bars*: 1 mm (A and B), 100 μm (C and D), 200 μm (E, F, M, and N), and 50 μm (G–L).

Discussion

The *Mamld1* mRNA expression was gradually and steadily increased from 12.5 to 18.5 dpc in the fetal testis of WT male mice. In this regard, intratesticular T has also been reported to increase in a similar manner in the mouse (10, 11). In addition, human study has also revealed clear *MAMLD1* expression in the fetal testis. These findings would argue for a positive role of *MAMLD1/Mamld1* in the T production in the fetal testis (1, 21).

We generated and studied *Mamld1* KO male mice. The results are summarized as follows: 1) mRNA levels of genes exclusively expressed in Leydig cells (*Star*, *Cyp11a1*, *Cyp17a1*, *Hsd3b1*, and *Insl3*) were mildly but significantly reduced, whereas those of genes expressed in other cell types or in Leydig and other cell types grossly remained normal (*Hsd17b3* is expressed in Sertoli cells of the fetal testis, although it is expressed in Leydig cells of the adult testis) (22, 23); 2) despite such mild reduction of mRNA levels, CYP17A1 and HSD3B proteins were sufficiently produced; 3) no demonstrable abnormality was identified by detailed studies for the external and internal genital regions; and 4) the *Mamld1* KO male mice retained normal fertility. Collectively, these findings imply that *Mamld1* deficiency reduces mRNA expression levels of multiple, if not all, genes expressed in mouse fetal Leydig cells but permits normal genital development and reproductive function. In support of this notion, such discrepancy between mRNA levels and protein levels as well as phenotypic consequences has been reported previously (24–26). Indeed, Greenbaum *et al.* (27) have proposed three possible explanations for the poor correlations between mRNA and protein expression levels: 1) there are many complicated and varied posttranscriptional mechanisms involved in turning mRNA into protein that are not yet sufficiently well defined; 2) proteins may differ substantially in their *in vivo* half lives; and 3) there may be a significant amount of error and noise in both protein and mRNA experiments that limit our ability to get a clear picture. These explanations would also apply to our results indicating normal expression of CYP17A1 and HSD3B proteins, in the presence of mildly but significantly reduced expression of *Cyp17a1* and *Hsd3b1* mRNAs. Furthermore, because CYP17A1 and HSD3B protein levels increased in a manner grossly similar to that reported for intratesticular T (10, 11) in both the *Mamld1* KO male mice and their WT littermates, this would be consistent with the apparently normal testicular function of the *Mamld1* KO male mice.

The normal phenotype in the *Mamld1* KO male mice is contrastive to the DSD phenotype in the *MAMLD1* mu-